Research Square

Preprints are preliminary reports that have not undergone peer review.
They should not be considered conclusive, used to inform clinical practice,
or referenced by the media as validated information.

Co-Delivery of Paclitaxel and Thymoquinone via Polymeric Nanoparticles Induces Apoptosis and Suppresses Epithelial-Mesenchymal Transition Through Wnt/β-Catenin Signaling in MCF-7 Breast Cancer Cell Line

Renuka Sharma
Guru Jambheshwar University of Science and Technology
Monika Verma
Guru Jambheshwar University of Science and Technology
Mandeep Kumar
Guru Jambheshwar University of Science and Technology
Rashmi Bhardwaj
Maharshi Dayanand University
Namita Singh
namitasingh71@gmail.com

Guru Jambheshwar University of Science and Technology

Research Article

Keywords: Paclitaxel, Thymoquinone, Co-loaded, Apoptosis, Nanoparticles, Epithelial-Mesenchymal Transition (EMT), Cytotoxicity, Migration

Posted Date: August 24th, 2026

DOI: https://doi.org/10.21203/rs.3.rs-10662907/v1

License: This work is licensed under a Creative Commons Attribution 4.0 International License.
Read Full License

Additional Declarations: No competing interests reported.

Co-Delivery of Paclitaxel and Thymoquinone via Polymeric Nanoparticles Induces Apoptosis and Suppresses Epithelial-Mesenchymal Transition Through Wnt/β-Catenin Signaling in MCF-7 Breast Cancer Cell Line

Renuka Sharma[1], Monika Verma[1], Mandeep Kumar[1], Rashmi Bhardwaj[2], Namita Singh[1]*

[1]Lab -202, Microbial Biotechnology Laboratory, Department of Biotechnology, Guru Jambheshwar University of Science and Technology, Hisar-125001, Haryana, India

[2] Maharshi Dayanand University, Rohtak-124001, Haryana, India

** Corresponding Author- namitasingh71@gmail.com, Contact- 9416928883*

Abstract

Combination nanotherapy is a promising strategy to overcome chemoresistance and improve therapeutic efficacy in breast cancer. In this study, polymeric nanoparticles co-loaded with paclitaxel (PTX) and thymoquinone (TQ) were prepared by the nanoprecipitation method and evaluated for their anticancer potential in MCF-7 breast cancer cell line. The nanoparticles of blank, PTX, TQ, and combined PTX-TQ showed mean particle sizes of 74.50 ± 42.69, 72.03 ± 33.31, 74.21 ± 42.99, and 134.1 ± 49.05, respectively, and all the nanoparticles had a Polydispersity Index (PDI) of approximately 0.2. Physiochemical characterization (FTIR, DSC, XRD, FESEM, and TEM) proved successful drug loading, spherical morphology, and amorphous drug dispersion. The combined PTX-TQ-NPs showed a strong cytotoxicity (IC_{50} = 2.442 ± 0.074 at 48 h) with synergistic interaction (CI= 0.78). All the nanoparticles suppressed colony formation. The wound healing and transwell assays revealed a reduction of ~85% and ~91% in migration, respectively. Flow cytometry revealed 48.41 ± 7.17% total apoptosis and significant G2/M arrest with 34.60 ± 0.55% sub-G1 accumulation. Nuclear fragmentation was confirmed using a DAPI stain. Real-time PCR and Western blot analysis showed a significant reversal of EMT with downregulation of β- catenin [0.005 ± 0.01-fold (RT-qPCR) and 0.591 ± 0.07(western blot)], N-cadherin, and Vimentin, and upregulation of E-cadherin (1.49 ± 0.06-fold). The results showed that combined PTX-TQ-NPs have synergistic effects against the MCF- 7 cancer cell via apoptosis induction, migration inhibition, and suppression of Wnt/ β-catenin signaling. The results suggest that PTX-TQ-NPs may be a promising nanotherapeutic platform for the management of breast cancer.

Keywords: Paclitaxel, Thymoquinone, Co-loaded, Apoptosis, Nanoparticles, Epithelial-Mesenchymal Transition (EMT), Cytotoxicity, Migration.

1 Introduction

The number of cases of cancer is increasing worldwide every single day. Breast cancer has emerged as a major health concern for women because of its high morbidity and death rate worldwide[1]. As of 2021, female breast cancer became the most prevalent cancer, accounting for 6.9% of overall tumor mortality. In 2022, breast cancer represented nearly 25% of newly diagnosed female cancers, with an annual incidence increase of about 0.6% as of 2023. Predictions suggest that breast cancer fatalities could reach around 1 million globally by 2030[2]. Despite various polychemotherapeutic treatments, hormonal therapies, surgical

interventions, and radiation therapies, only one-third of breast cancer patients obtain effective treatments[3]. Breast cancer treatment frequently uses combination therapy to maximise therapeutic efficiency and minimise adverse effects. Advanced tumors often use combination treatment as an effective technique to overcome multi-drug resistance (MDR) effects[4,5]. To overcome these barriers in breast cancer treatment, it is necessary to establish an appropriate drug delivery system that can effectively transport medicinal products to the tumor site, enhancing their efficiency and biosafety.

Paclitaxel (PTX), extracted from the bark of the Pacific yew tree, Taxus brevifoliya, is among the often-recommended conventional chemotherapeutic agents for various malignancies [6]. Paclitaxel (Taxol™) is used in the treatment of several malignancies, including breast, ovarian, cervical, pancreatic, and lung cancers [7,8]. PTX inhibits the depolymerization of microtubules in tumor cells, leading to cell cycle arrest during mitosis and subsequent induction of death[9]. PTX is usually mixed in a vehicle consisting of a 1:1 mixture of Cremophor EL and ethanol before delivery. The harmful effects of Cremophor EL have been seen in both animal models and human beings. Furthermore, PTX may eliminate actively proliferating normal cells, hence leading to harmful side effects[10]. A study of PTX and Curcumin nanoparticles against MCF-7 cells in vitro and vivo using PCEC polymer demonstrated that PTX-CUR-NPs induced cytotoxicity, arrested the cell cycle at G2/M phase, inhibited tumor growth in vivo, extended mice survival, reduced tumor tissue glucose metabolism, and exhibited lower toxicity[11]. In another study, a combination of PTX and quercetin nanoparticles induced apoptosis, necrosis, and tumor growth inhibition by downregulating P-gp expression and inhibiting the efflux of cellular PTX, which eventually inhibited mitosis in G2/M phase of the cell cycle[12].

Apart from PTX, thymoquinone (TQ: 2-isopropyl-5 methylbenzo-1,4-quinone) a quinone-based phytochemical, is the main active constituent of the *Nigella sativa* plant[13]. *Nigella sativa* is one of the most popular herbs that grows in the Mediterranean and in Western Asian areas is a medicinal plant belongs to *Ranunculaceace* family. The plant has been used for centuries in Asia, Africa, and Europe for the treatment of many diseases like asthma, skin irritation, hypertension, inflammation, and gastrointestinal conditions[14]. *Nigella sativa* is also known as black cumin and kalonji[15]. TQ has many pharmacological properties like anticancer, anti-inflammatory, antimicrobial, antioxidant, antihistamic, immunomodulatory etc.[16]. TQ induces antiproliferative and pro-apoptotic effects through various distinct pathways: a disruption of intracellular redox balance via reactive oxygen species (ROS) production, upregulation of the pro-apoptotic effector gene Bax, transcriptional and translational downregulation of the anti-apoptotic gene Bcl-2, inhibition of the NF-κB pro-survival transcriptional pathway, and direct activation of capase-9/3 intrinsic apoptotic cascade. In addition to its direct cytotoxic effects, TQ enhances the anticancer effectiveness of many recognized chemotherapeutic agents, including gemcitabine, tamoxifen, and doxorubicin, through synergistic pathways in breast cancer cell models[17,18].

Epithelial-mesenchymal transition (EMT) is the transcriptional reprogramming through which carcinoma cells exchange their epithelial adhesive identity for a mesenchymal, migratory, and invasive phenotype. This process is a crucial molecular basis of breast cancer metastatic proliferation, stem tissue acquisition and resistance to cytotoxic chemotherapy in breast cancer. The classical Wnt/β-catenin signalling pathway is a master regulator of breast cancer EMT: in the presence of aberrantly activated Wnt, β-catenin escapes proteasomal degradation by the APC/Axin/GSK-3β destruction complex, translocate to the nucleus and interacts with

TCL/LEF transcription factor to activate downstream targets that drives EMT including Snail, cyclin D1, matrix metalloproteins(MMP-2, MMP-7, MMP-9) and the mesenchymal adhesion molecule N-cadherin[19,20]. TGF-β1 enhances Wnt-induced epithelial-mesenchymal transition (EMT) via Smad2/3-mediated transcriptional activation of Wnt ligands and direct suppression of the epithelial junctional protein E-cadherin, therefore establishing an autocrine signaling loop that maintains the mesenchymal phenotype[21]. Therapeutically targeting this oncogenic axis presents a promising technique to concurrently inhibit tumor invasion, metastatic dissemination, and chemoresistance[22]

Despite all these pharmacological properties, PTX and TQ are both less soluble in water[10,18]. Considering these limitations and the benefits of combination therapy, developing a new drug delivery method for the simultaneous administration of PTX and TQ may be a useful strategy for cancer treatment. Fortunately, polymer chemistry and nanotechnology provide a potential alternative for the development of effective drug delivery systems capable of demonstrating efficient combination treatment[23]. A wide range of research has revealed that nanoparticles provide significant benefits for cancer treatment, including prolonged drug release, targeted delivery to cancer cells, and enhanced bioavailability. Simultaneously, polymeric nanoparticles possess many advantages in drug delivery systems. They have little risk of immunogenicity and disease transmission and demonstrate great stability in systemic circulation[24].

Eudragit RS 100 is a water-insoluble, pH-independent copolymer of ethyl acrylate, methyl methacrylate, and a low proportion (~5%) of trimethyl ammonium ethyl methacrylate chloride functional groups, which has emerged as a versatile pharmaceutical polymer for sustained-release nanoparticulate drug delivery[25]. The quaternary ammonium substituents confer a net cationic charge to the polymer backbone, which has been exploited for enhancing nanoparticle-cell membrane interaction, mucoadhesion, and intracellular retention in several oncology drug delivery investigations[26]. Nanoprecipitation of Eudragit RS 100 in the presence of Poloxamer 188, a non-ionic triblock copolymer surfactant composed of a central hydrophobic polypropylene oxide block flanked by hydrophilic polyethylene oxide chains, yields nanoparticles with controlled particle size, improved colloidal stability, and reduced opsonisation-mediated reticuloendothelial clearance, while Poloxamer 188 additionally exerts a recognised P-glycoprotein inhibitory effect that may further potentiate intracellular retention of P-gp substrate drugs such as PTX[27,28]. Poloxamer 188, also known as Pluronic F68, and FDA-approved[29].

Although individual anticancer attributes of PTX and TQ are well-documented, the mechanistic consequences of their Eudragit RS 100 nanoparticle co-delivery on the Wnt/β-catenin/EMT regulatory axis in MCF-7 breast cancer cells have not been systematically characterised. To address this gap, the present study aimed to: synthesize and comprehensively characterise PTX-TQ-NPs by particle size analysis (PSA), zeta potential, PDI, FESEM, TEM, FTIR, DSC, and XRD; and further evaluate their in vitro anticancer mechanistic profile through cell viability (MTT), colony formation, wound healing, transwell migration, Annexin V-FITC/PI apoptosis, cell cycle, DAPI nuclear staining, and EMT gene and protein expression assays (RT-qPCR and Western blot), with mechanistic focus on the Wnt/β-catenin//EMT signalling.

2 Results

2.1. Preparation and Characterizations of Nanoparticles

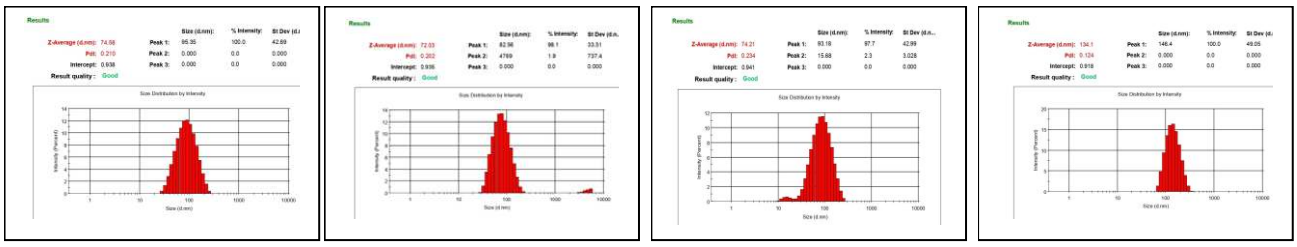
2.1.1. Particle Size, PDI, Zeta Potential and Morphology

In the current study, Blank, PTX, TQ, and PTX-TQNPs were synthesized successfully via the nanoprecipitation method. After preparation, the NPs were stored in dark amber reagent bottles because of the phytochemical nature of TQ for further use and lyophilized for characterization. Characterization of the synthesized NPs, including particle size analysis, zeta potential, and polydispersity index, was performed using dynamic light scattering. The size distributions of all four different types of NPs were illustrated in Figure 1 (A). The corresponding average diameters of Blank NPs were 74.50 ± 42.69, PTX NPs were 72.03 ± 33.31, TQ NPs were 74.21 ± 42.99, and PTX-TQ-NPs were 134.1 ± 49.05. The PDI of all NPs was ~ 0.2. Table 1 indicates that all of four NPs exhibit a size below 200 nm and the narrowest PDI distribution. Combined NPs of PTX and TQ exhibit a large particle size as compared to others. To examine the stability of all the NPs, the zeta potentials were determined in Figure 1 (B). Table 1 indicates that all four NPs are positively charged. Among all four NPs, PTX NPs exhibited a high zeta potential of 32.4 ± 6.79. FESEM and TEM analysis verified that the particles exhibited a spherical morphology with a monodispersed size distribution across all kinds of nanoparticles [Figure 1 (C and D)].

Table 1 Physiochemical characterizations of Nanoparticles

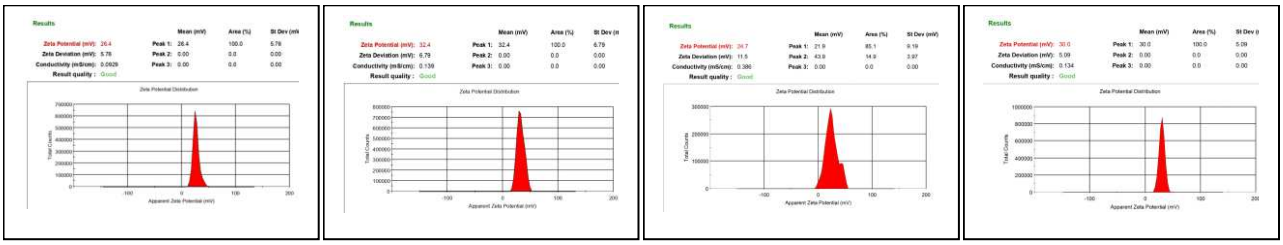
Formulations	Size	PDI	Zeta Potential	Encapsulation Efficiency%	Drug Loading %
Blank-NPs	74.50 ± 42.69	0.210	26.04 ± 5.76	-	-
PTX-NPs	72.03 ± 33.31	0.202	32.4 ± 6.79	87.60%	15.92%
TQ-NPs	74.21 ± 42.99	0.234	24.7 ± 9.19	93.34%,	18.06%,
PTX-TQ-NPs	134.1 ± 49.05	0.124	30.0 ± 5.09	77.10%(PTX) 81.22% (TQ)	7.01%(PTX) 7.42% (TQ)

A



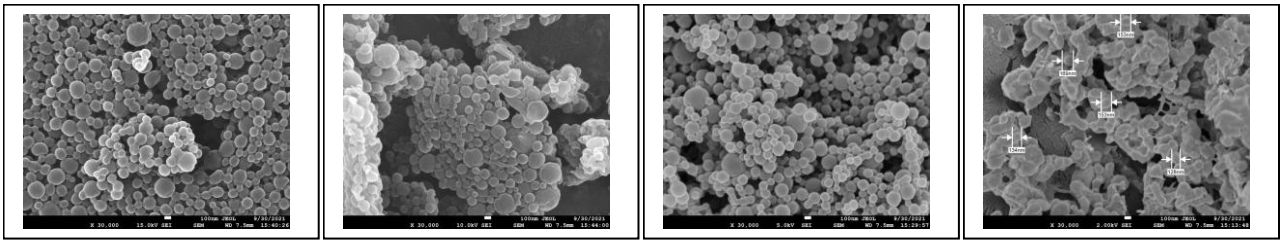
a **b** **c** **d**

B



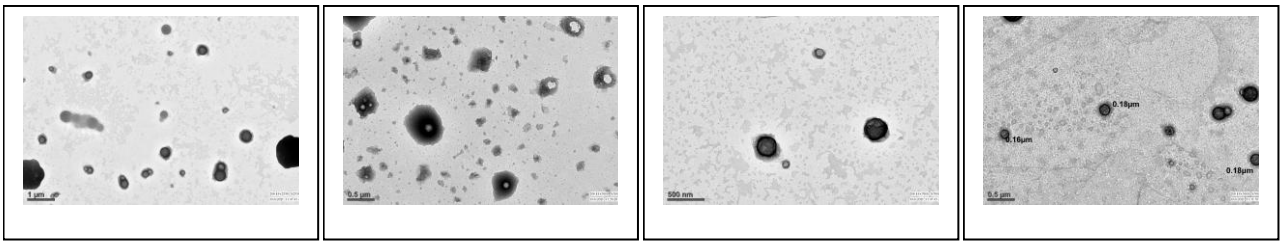
a b c d

C



a b c d

D

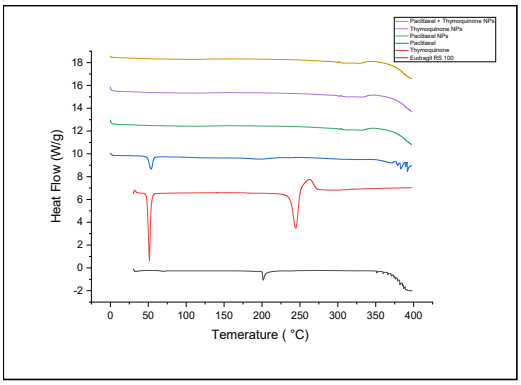


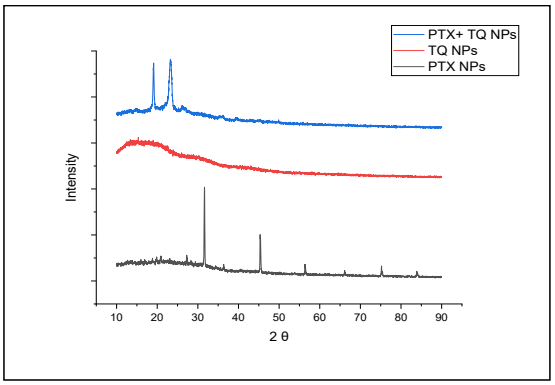
a b c d

Fig 1 (A) represents particle size distribution (a) Blank, (b) PTX, (c) TQ, and (d) PTX-TQ-NPs. (B) zeta potential of (a) Blank, (b) PTX, (c) TQ, and (d) PTX-TQ-NPs. (C) FESEM of (a) Blank, (b) PTX, (c) TQ, and (d) PTX-TQ-NPs. (D) TEM of (a) Blank, (b) PTX, (c) TQ, and (d) PTX-TQ-NPs.

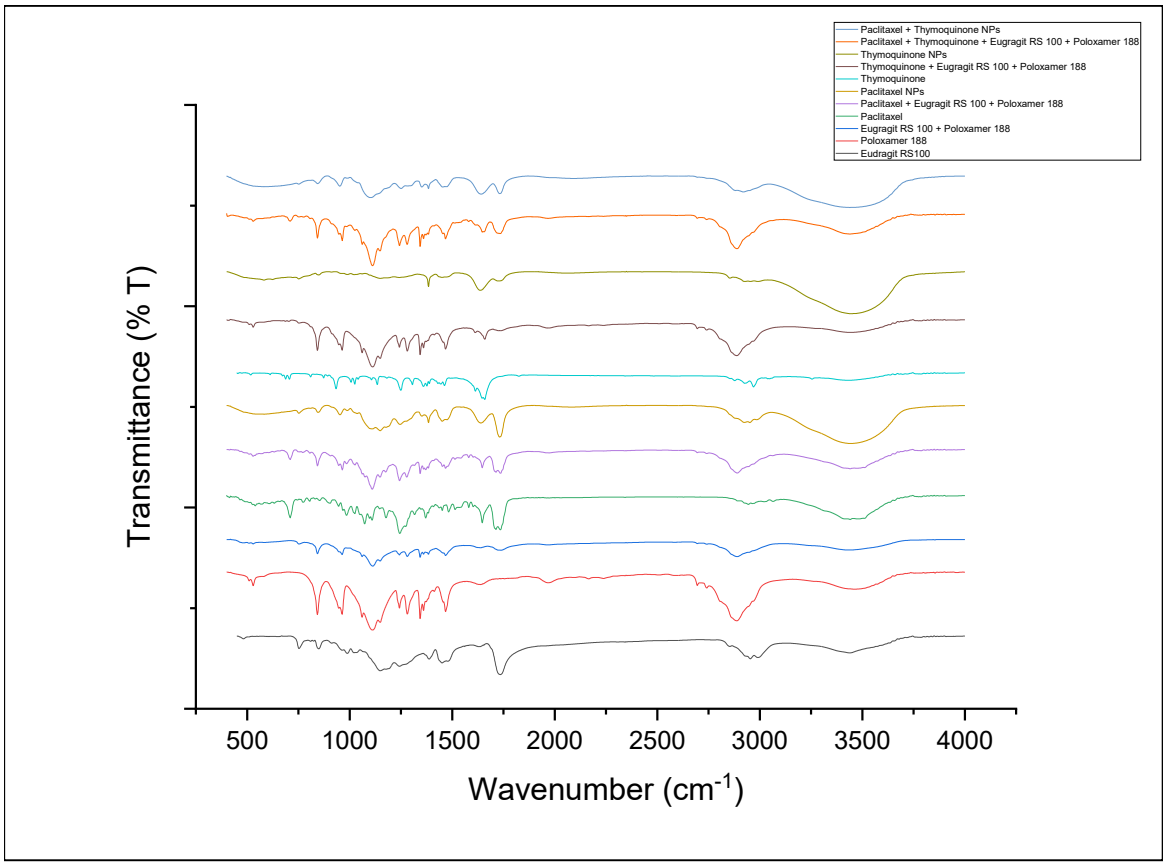
2.1.2 Differential Scanning Calorimetry and X-Ray Diffraction Analysis

The physical state of all the nanoparticles was evaluated using differential scanning calorimetry and X-ray diffraction. The DSC of free PTX, free TQ, Eudragit RS 100, and nanoparticles is shown in Figure 2 (a). Thermal analysis is an effective method for evaluating the dispersion of solute particles inside a polymeric matrix. PTX and TQ exhibit distinct melting endothermic peaks at 244.95 °C and 53.58 °C, respectively. The absence of these distinctive peaks in nanoparticles indicates that PTX and TQ are molecularly scattered within the polymeric matrix, that further confirms the entrapment of PTX and TQ in nanoparticles. The X-RD analysis of all nanoparticles indicates a molecular dispersion or an amorphous nanodispersion with the polymeric matrix of the nanoparticles [Figure 2 (b)].





a **b**



c

Fig 2 represents the physicochemical characterization of nanoparticles a) DCS of Eudragit RS 100, free PTX, TQ, PTX-NPs, TQ-NPs, and PTX-TQ-NPs. b) X-Ray Diffraction of PTX, TQ and PTX-TQ nanoparticles. c) FTIR spectrum of Eudragit RS 100, Poloxamer 188, mixture of Eudragit RS100 and Poloxamer 188, free PTX, mixture of free PTX, Eudragit RS100 and Poloxamer 188, PTX-NPs, free TQ, mixture of Free TQ, Eudragit RS100 and Poloxamer 188, TQ-NPs, mixture of PTX, TQ, Eudragit RS100 and Poloxamer 188, and PTX-TQ-NPs.

Figure 2 (c) shows the FTIR spectra of free PTX, free TQ, Eudragit RS100, poloxamer 188, mixture of PTX and TQ, their mixture, and all nanoparticles. The FTIR spectrum of pure PTX displayed characteristic absorption at 3440.74 cm^{-1}(N-H/O-H stretching), 2944.59 cm^{-1} (aliphatic C-H asymmetric stretch), 1734.59 cm^{-1} (ester C=O stretch). Pure TQ exhibited bands

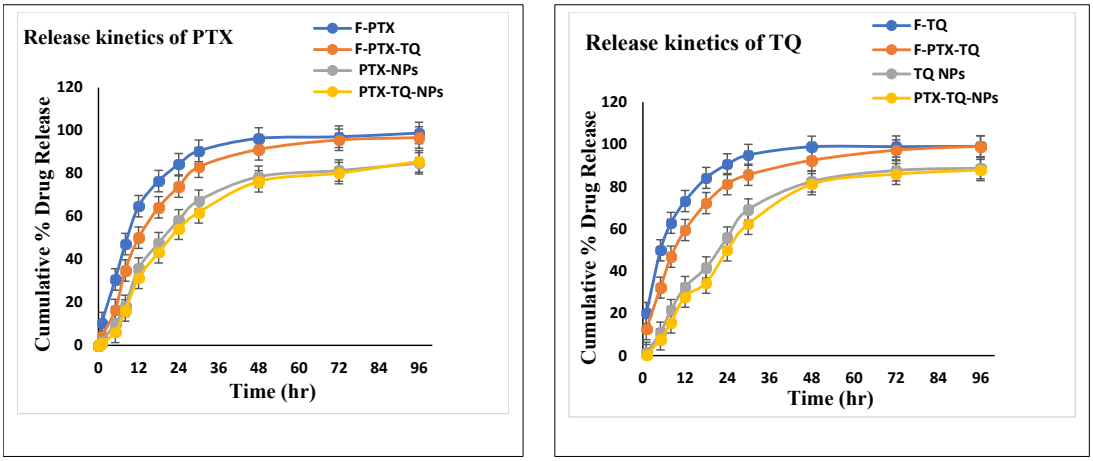
at 2969.34 cm^{-1} (aliphatic C-H), 1658.87 cm^{-1}(quinone C=O conjugated stretch), and 1462.48 cm^{-1} (C-H bending). Eudragit RS 100 displayed characteristic absorption at 1736.14 cm^{-1} (ester C=O of the methylacrylate backbone) and a weak band near 1450cm^{-1} attributable to the quaternary ammonium trimethylammonioethyl substituent. The FTIR spectrum of PTX-TQ-NPs retained all principal characteristics absorption bands of PTX and TQ, confirming complete molecular integrity of both drugs following the nanoprecipitation process. Notably, the PTX ester carbonyl band at 1734.59 cm^{-1} exhibited a bathochromic shift of 1731.83 cm^{-1} and the TQ quinone C=O at 1658.87 cm^{-1} shifted by 1640.79 cm^{-1} in the nanoparticle spectrum, attributable to hydrogen bonding and electrostatic/hydrophobic drug-Eudragit RS 100 non-covalent interactions. This potentially including ion-dipole interaction between the cationic quaternary ammonium groups of the polymer and electronegative carbonyl/quinone oxygen atoms of the encapsulated drugs, driving drug retention within the polymeric core[24]. Crucially, no new absorption bands appeared, and no characteristic peaks were eliminated, unambiguously confirming the absence of covalent chemical bond formation or deleterious drug-polymer incompatibility between co-encapsulated PTX, TQ, and the Eudragit RS 100 matrix. After analysing the FTIR spectra of all the nanoparticles, it was observed that they closely resemble their respective coating polymer which was Eudragit RS 100. This signifies the absence of chemical interactions between the polymer and the drugs. These findings indicate that the FTIR distinctive peaks of PTX and TQ are masked when encapsulated individually as well as in combination.

2.2.Entrapment efficiency and Drug loading

The entrapment efficiencies and drug loading of PTX, TQ, and PTX-TQ NPs were evaluated using UV-vis spectroscopy and are shown in Table 1. The entrapment efficiencies of PTX and TQ NPs were calculated to be 87.60% and 93.34%, respectively. The entrapment efficiencies of PTX and TQ in combined nanoparticles were calculated to be 77.10% and 81.22%, respectively. Results indicate that the majority of PTX and TQ were entrapped in nanoparticles. The drug loading for individual formulations, PTX and TQ nanoparticles, was 15.92% and18.06%, respectively. In the combined formulations, the drug loading of PTX and TQ nanoparticles was 7.01% and 7.42%, respectively.

2.3 In vitro release

The release profiles of PTX, TQ, and PTX-TQ-NPs indicated continuous release of PTX and TQ from the polymeric matrix at a physiological pH of 7.4 in phosphate buffer at 37 °C. Both PTX and TQ nanoparticles exhibited an immediate burst release within 24 hours, followed by a continuous release from the polymeric matrix. Approximately 58.22 ± 0.94 % and 54.28 ± 0.97 % of PTX was released from PTX-NPs and PTX-TQ-NPs after 24 hours, respectively, whereas 55.86 ± 0.88 % and 49.84 ± 0.99 % of TQ was released from the TQ-NPs and PTX-TQ-NPs within the same time frame, respectively (Fig. 3). In contrast, PTX and TQ from F-PTX, F-TQ, and F-PTX-TQ showed immediate release.



a **b**

Fig. 3 (a) In vitro cumulative release profile of PTX from F-PTX, F-PTX-TQ, PTX-NPs, and PTX-TQ-NPs. (b) In vitro cumulative release profile of TQ from F-TQ, F-PTX-TQ, TQ-NPs, and PTX-TQ-NPs.

2.4 Cell viability

The viability of MCF-7 breast adenocarcinoma cells was assessed using the MTT colorimetric proliferation assay. The cytotoxic behaviour of free paclitaxel (F-PTX), free thymoquinone (F-TQ), F-PTX with fix concentration of F- TQ, blank nanoparticles, PTX-NPs, TQ-NPs, PTX-NPs with fix concentration of TQ-NPs, and combined PTX-TQ-NPs was systematically examined over a wide concentration gradient and at three time intervals (24, 48, and 72 hours). All formulations showed concentration- and time-dependent antiproliferative activity, and the cytotoxic potency was gradually enhanced with an increase in drug concentration as well as exposure duration, as shown in Figure 4. F-PTX showed potent antiproliferative activity against MCF-7 cells, with an IC_{50} of 0.56 ± 0.08 µg/ml (48 h), in agreement with previously reported PTX IC_{50} values of 0.2 ± 0.07 µM in MCF-7 cells at 48 hours [30]. F-TQ showed moderate cytotoxic potency with an IC_{50} value of 10.41 ± 0.85 µg/ml (48 h), which is consistent with the reported IC_{50} of 64.93 ± 14 µM for TQ against MCF-7 cells at 24 hours[30]. F-PTX showed greater cytotoxicity than free PTX, with IC_{50} values of 0.247 ± 0.019 µg/ml (48 h) in combination with 4 µg/ml F-TQ.

PTX-NPs showed potent antiproliferative activity against MCF-7 cells, with IC_{50} values of 0.37 ± 0.07 (48 h). TQ-NPs showed moderate cytotoxic potency, with IC_{50} values of 7.06 ± 0.76 µg/ml (48 h). PTX-NPs showed greater cytotoxicity than individual PTX nanoparticles, with IC_{50} values of 0.085 ± 0.022 µg/ml (48 h) when combined with 4 µg/ml TQ-NPs. Combined PTX-TQ-NPs showed greater cytotoxicity than the individual nanoparticles, with IC_{50} values of 2.44 ± 0.07µg/ml (48 h). IC_{50} values for all treatments are shown in Table 2 at different time intervals.

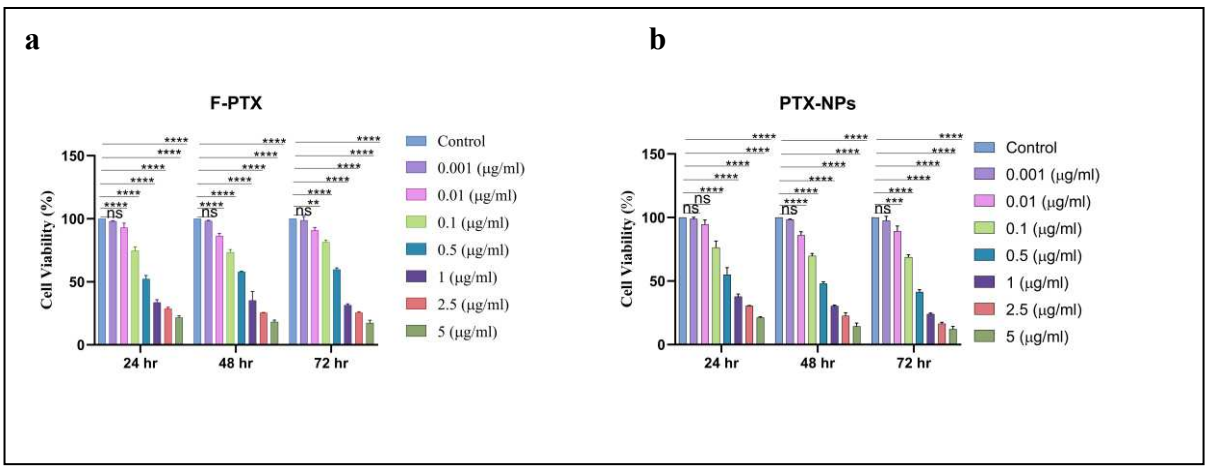
Combined PTX-TQ-NPs demonstrated significantly superior antiproliferative potency than free treatments and individual PTX and TQ nanoformulations at all time points assessed with IC_{50} values at 24, 48, and 72 h (Table 2). The Chou-Talalay combination index (CI) analysis was performed to calculate the CI value at the IC_{50} effective dose level, using the following equation

$$CI = \frac{IC50\ of\ Drug\ X\ in\ Combination}{IC50\ od\ Drug\ X\ Alone} + \frac{IC50\ od\ Drug\ Y\ in\ Combination}{IC50\ of\ Drug\ Y\ Alone}$$

Following Chou and Talalay, drug–drug interactions were evaluated using the Combination Index (CI), where CI < 1 denotes synergism, CI = 1 denotes additivity, and CI > 1 denotes antagonism; CI values were calculated across effect levels (fraction affected, fa) to characterize effect-dependent interaction profiles. The CI of PTX and TQ nanoparticles and F-PTX and F-TQ was 0.78 and 0.82, which was found to be preferably < 1, thus establishing the synergistic pharmacological interaction between co-encapsulated PTX and TQ[31]. Such synergism is most likely due to the temporally coordinated intracellular release of both agents from the shared nanocarrier, enabling simultaneous engagement of their complementary, mechanistically convergent pro-apoptotic targets in the same cell[28]. These results suggest that the combination therapy of nano-encapsulated PTX-TQ is significantly more effective than the individual free drugs and individual nanoparticles, which is consistent with similar synergistic effects of bazedoxifene-PTX combinations against MCF-7 cells[32]. Importantly, blank nanoparticles devoid of the active pharmaceutical ingredients exhibited minimal cytotoxicity only when used in high concentration, indicating that the antiproliferative activities were solely due to the encapsulated therapeutic agents and not the polymeric carrier. The effect of Blank NPs and DMSO on MCF-7 cells is shown in Supplementary Fig. 1.

Table 2. IC_{50} values for all formulations at different time intervals.

Formulations	**24 h(µg/ml)**	**48 h(µg/ml)**	**72 h(µg/ml)**
F-PTX	0.45 ± 0.03	0.56 ± 0.08	0.60 ± 0.02
PTX-NPs	0.52 ± 0.13	0.37 ± 0.06	0.31 ± 0.01
F-TQ	10.10 ± 0.42	10.41 ± 0.85	11.67 ± 0.97
TQ-NPs	8.25 ± 0.26	7.06 ± 0.76	6.83 ± 0.10
F-PTX+ 4 µg/ml F-TQ	0.36 ± 0.85	0.24 ± 0.01	0.24 ± 0.06
PTX-NPs+ 4 µg/ml TQ-NPs	0.15 ± 0.01	0.08 ± 0.02	0.09 ± 0.05
PTX-TQ-NPs	2.69 ± 0.13	2.44 ± 0.07	2.23 ± 0.11



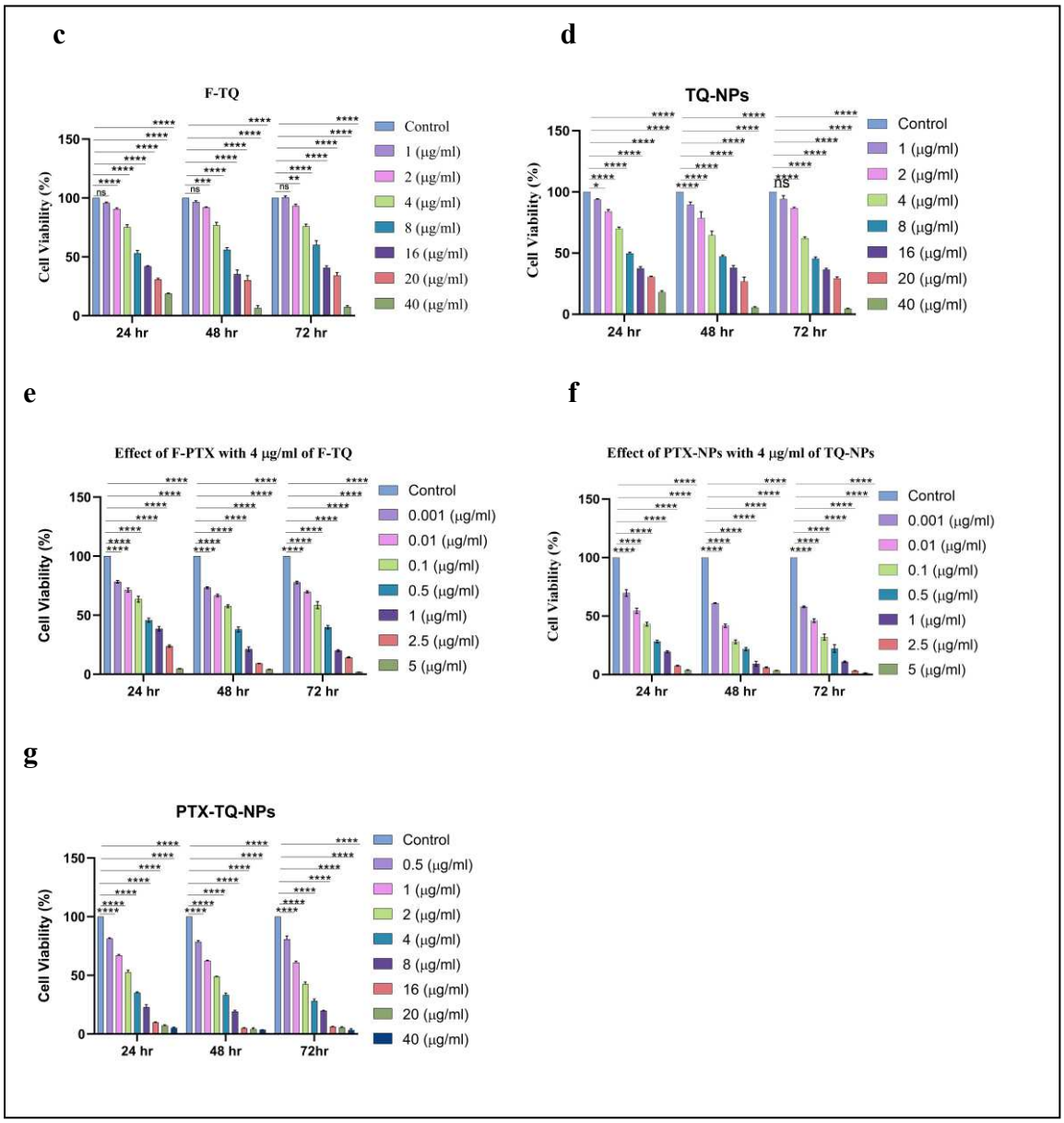


Fig 4 The graphical representation of cytotoxic (a) effect of F-PTX on the viability of MCF-7 breast cancer cells. Cell viability was determined by the MTT assay as described in the methods section. Cell viability was assessed in MCF-7 cells after treatment with various concentrations of PTX. (b) Cell viability was assessed in MCF-7 cells after treatment with PTX-NPs. (c) Effect of F-TQ on the viability of MCF-7 breast cancer cell lines. (d) Effect of TQ-NPs on the viability of MCF-7 breast cancer cells. (e) Effect of F-PTX on the viability of MCF-7 breast cancer cells with 4 µg/ml F-TQ. (f) Effect of PTX-NPs on the viability of MCF-7 breast cancer cells with 4 µg/ml TQ-NPs. (g) Effect of combined PTX-TQ-NPs on the viability of MCF-7 breast cancer cells. Significance values were compared to control: *$p < 0.05$, **$p < 0.01$, ***$p < 0.001$. All data are shown as the mean ± SD from three independent experiments

2.5 Colony Formation Assay

The MTT assay evaluates short-term metabolic inhibition, whereas clonogenic survival assays assess long-term regenerative capability, which is most closely associated with the likelihood

of tumor recurrence. Following a 48-hour exposure to the drugs at IC_{50} values and below IC_{50}, the MCF-7 cells (500 cells per well) were monitored for 15 days, and subsequently, the colonies were enumerated. Untreated controls exhibited an average of 1145.66 ± 125.70 colonies/well. The MCF-7 cells failed to form colonies in the presence of all nanoparticles at their IC_{50} values, but some colonies formed at concentrations below IC_{50}. The Colony formation efficiencies were calculated for all the nanoparticles by considering the control CEF as 100%. The calculated CEF for MCF-7 decreased by about 34% in the presence of PTX-NPs (0.05 µg/ml) and 29% in the presence of TQ-NPs (2 µg /ml). The MCF-7 cells fail to form colonies in the presence of all the concentrations of PTX-TQ NPs.

Crystal violet photographs confirmed the counts, revealing visibly sparse and structurally compromised colonies in nanoparticle wells, in contrast to the dense, well-formed aggregates observed in untreated wells, as shown in Figure 5. This significant long-term suppression indicates that the co-loaded nanoparticles affect both the actively proliferating bulk population and the slower-cycling, therapy-resistant reservoir that sustains tumor regeneration.

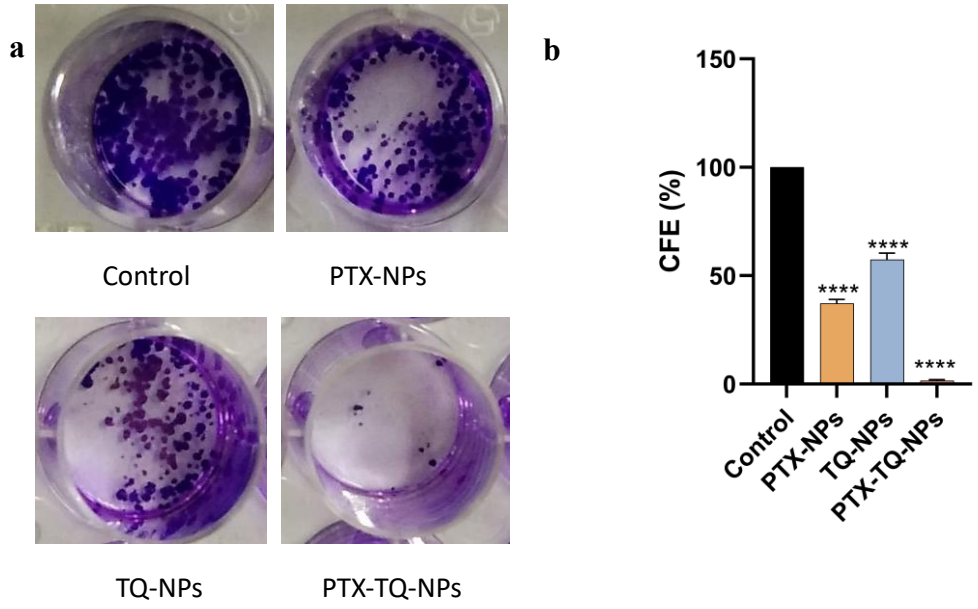


Fig.5 a) shows the colony formation inhibition of MCF-7 cells by all the nanoparticles compared to control; b) quantitative analysis of the colony formation efficiency percentage (CFE%) compared to control. Significance values were compared to control: *$p < 0.05$, **$p < 0.01$, ***$p < 0.001$. All data are shown as the mean ± SD from three independent experiments

2.6 Wound Healing (Scratch) Assay

A wound healing assay was conducted to assess the impact of PTX-NPs, TQ-NPs, and PTX-TQ-NPs on the migratory ability of MCF-7 cells. The untreated control group showed the fastest wound healing of the scratch area closure within 48 h. Whereas cells subjected to nanoparticle formulations exhibited a significant reduction in migration rate.

After 24 h, PTX-NPs showed wound closure of about 58% (at concentration 0.05 µg/ml) and about 35% at IC_{50}, while TQ-NPs showed 62% (at concentration 2 µg/ml) and 48% at IC_{50}. The

PTX-TQ-NPs exhibited the most significant closure rate, about 24% (at con. 2 µg/ml) and about 5% at IC_{50} . At 48 h, wound healing in the control group was almost complete (~85%), whereas PTX nanoparticle-treated cells exhibited ~73% (at concentration 2 µg/ml) and ~64% at IC_{50} , and TQ nanoparticle-treated cells exhibited ~71% (at con. 2 µg/ml) and ~52% at IC_{50} . The PTX–TQ-NPs combination limited closure to ~45% (at a concentration of 1 µg/ml) and ~10% at IC_{50} , suggesting a prolonged inhibition of migratory activity, as shown in Figure 6 (a). The quantitative study of wound closure % demonstrated that the combined nanoparticle formulation markedly reduced cell migration in comparison to individual treatments (Figure 6 b).

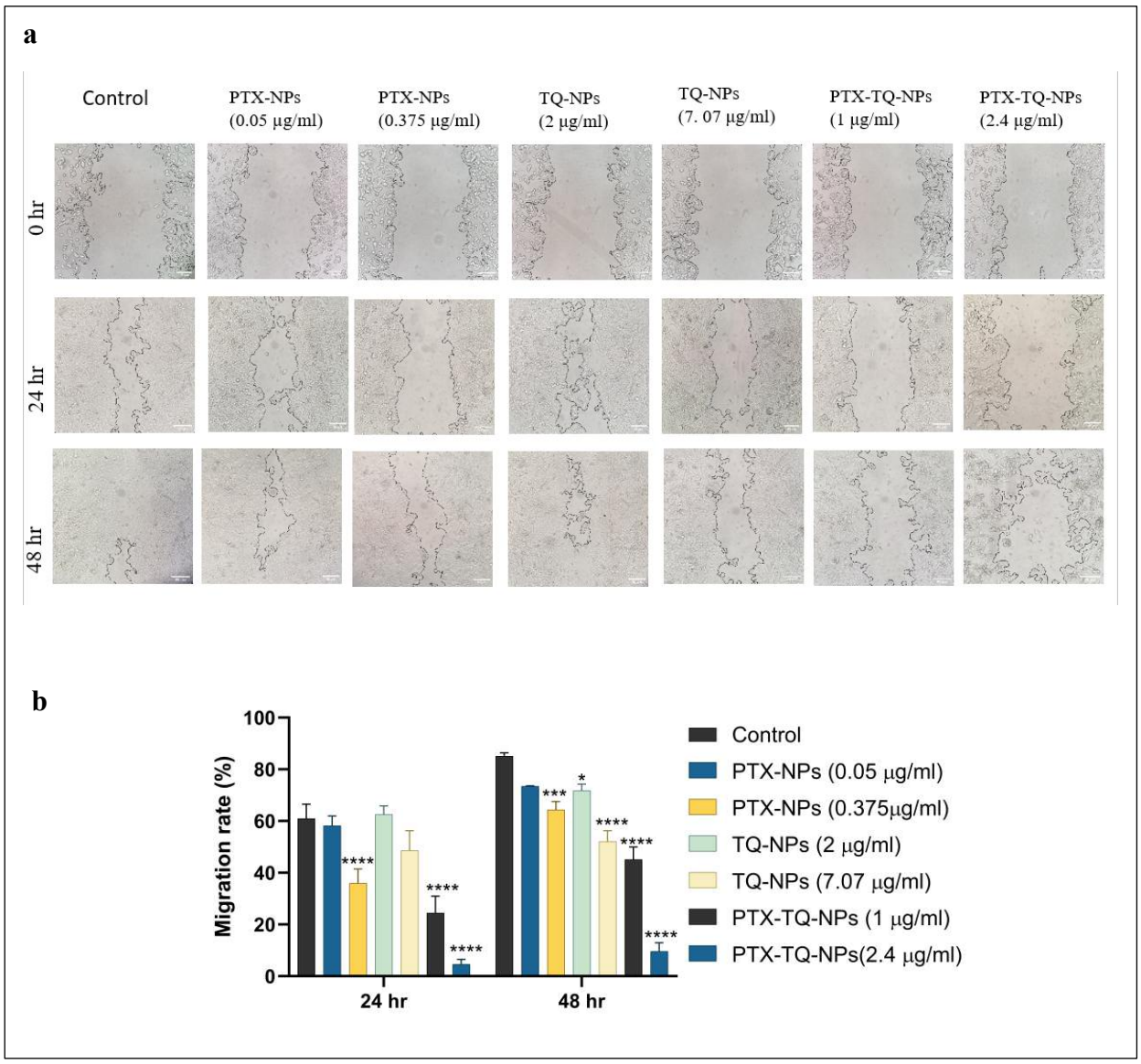


Fig. 6 represents the anti-migratory effect of all nanoparticles on MCF-7 cells. (a) The pictorial representation of the wound healing assay illustrating the rate of migration of MCF-7 cells upon treatment of different doses of PTX-NPs, TQ-NPs, and PTX-TQ-NPs at 0, 24 h and 48 h of incubation. (b) The graphical representations of the percent cell migration rate of MCF-7 cells. Significance values were compared to control: *$p < 0.05$, **$p < 0.01$, ***$p < 0.001$. All data are shown as the mean ± SD from three independent experiments.

2.7 Transwell Migration Assay

The transwell migration assay demonstrated a marked reduction in the migratory capacity of MCF-7 cells following nanoparticle treatment. Compared to the untreated control group, all nanoparticle formulations significantly inhibited cell migration; however, the combined PTX-TQ nanoparticles produced the most pronounced effect (Figure 7 a). The quantitative analysis revealed that PTX-TQ-NPs reduced the number of migrated cells by ~91% in 48 h, indicating a strong suppression of metastatic behaviour. In contrast, PTX-NPs and TQ-NPs showed ~78% and ~ 48% inhibition in 48 h (Figure 7 b). The substantial decrease in migrated cells in the PTX-TQ-NP group suggests that the synergistic formulation effectively disrupts cellular motility, likely through EMT reversal and downregulation of migration-associated proteins such as MMP-9, N-cadherin, and Vimentin. These findings confirm that PTX-TQ-NPs significantly impair the invasive potential of breast cancer cells.

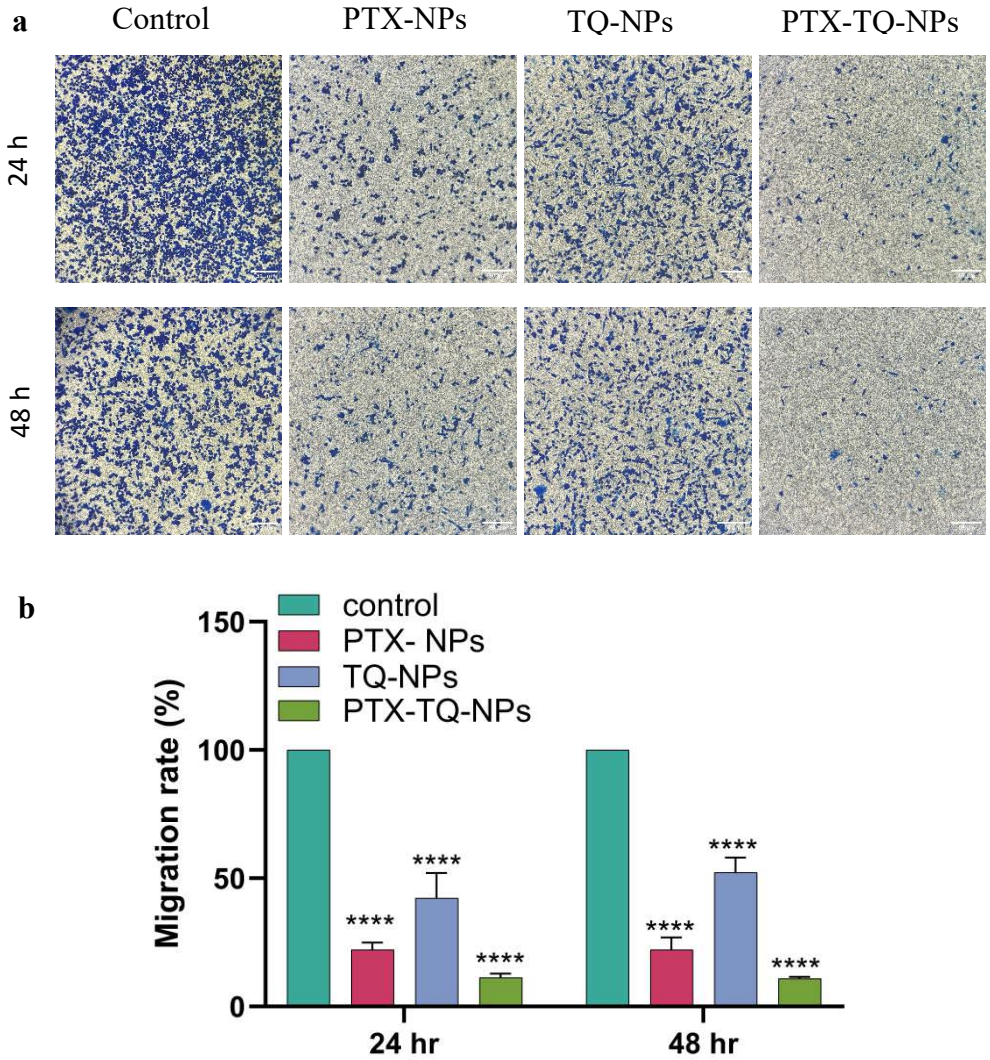


Fig. 7 represents the anti-migratory effect of all nanoparticles on MCF-7 cells. (a) The pictorial representation of the transwell assay illustrating the rate of migration of MCF-7 cells upon treatment of different doses of PTX-NPs, TQ-NPs and PTX-TQ-NPs at 24 h and 48 h of incubation. (b) The graphical representations of the percent cell migration rate of MCF-7 cells.

Significance values were compared to control: *p < 0.05, **p < 0.01, ***p < 0.001. All data are shown as the mean ± SD from three independent experiments.

2.8 Apoptosis analysis via Flow cytometry

The apoptosis of MCF-7 breast cancer cells was assessed with flow cytometric analysis using Annexin V-FITC/PI dual staining. Untreated control MCF-7 cells exhibited elevated viability, with a baseline total apoptotic fraction of 13.62 ± 4.56% and negligible necrosis 3.57 ± 0.62%. PTX-NPs and TQ-NPs demonstrated dose-dependent enhancements with total apoptosis of 28.53 ± 4.62% and 23.22 ± 11.65%, respectively, indicating the apoptotic superiority of nanoencapsulation compared to the untreated control.

The PTX-TQ-NPs exhibited markedly elevated apoptosis, with total apoptosis of cells at 48.41 ± 7.17%, comprising early apoptotic (Q3: 10.21 ± 3.37%) and late apoptotic (Q2: 38.20 ± 4.00%) subpopulations, while necrotic events were confined to 24.16 ± 2.48. The results showed that most of the cells died through a controlled, caspase-dependent apoptotic process rather than through inflammatory necrosis ($p < 0.001$ vs. all groups). The dot plot (Figure 8 a) clearly illustrates a shift in cell population from early apoptosis to late apoptosis as treatment strength increases. The combined treatment triggers a strong apoptotic effect because PTX and TQ activate the same mitochondrial death pathway from different angles: PTX causes mitotic arrest and promotes cytochrome-c release, while TQ increases Bax and reduces BCl-2 levels. Together, they overpower the cell's survival mechanism and strongly promote mitochondrial-mediated apoptosis[33].

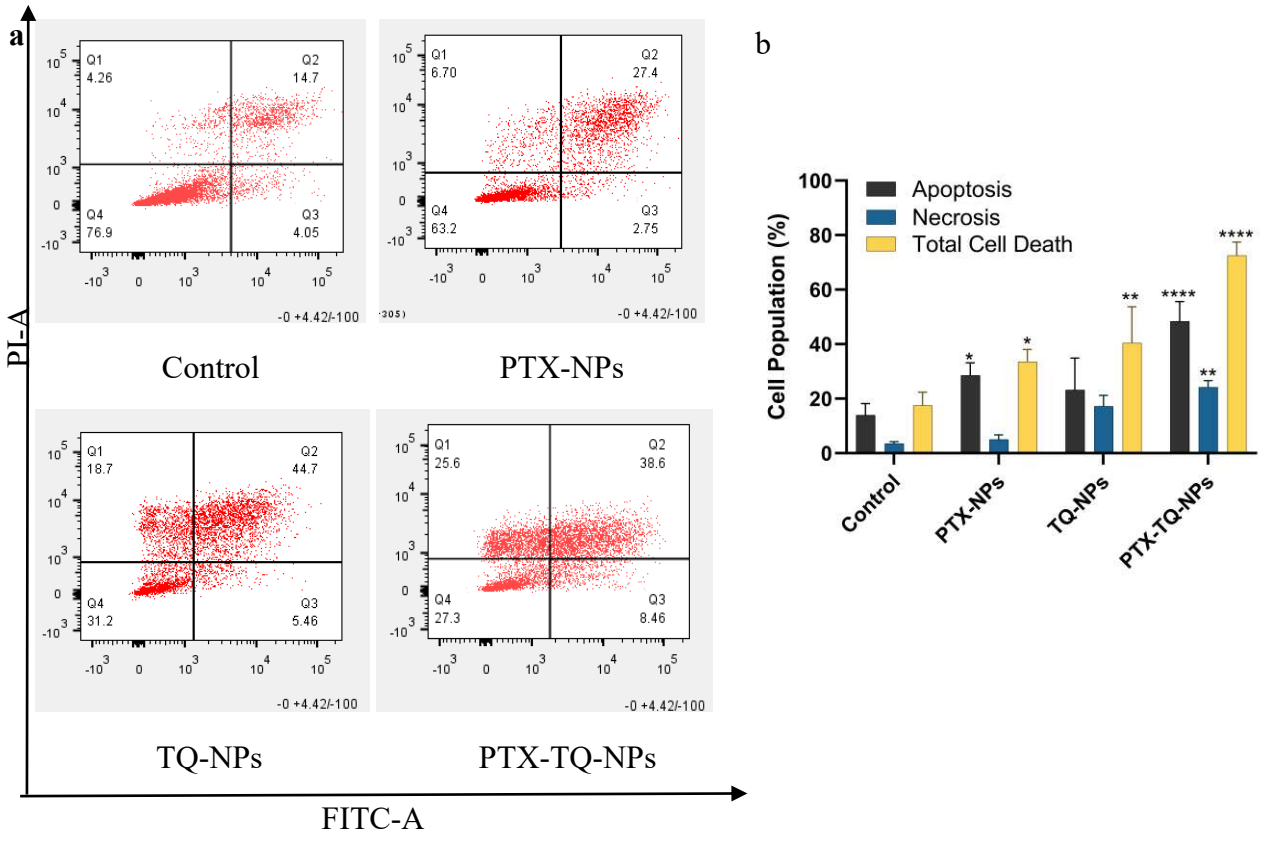


Fig. 8 (a) Represents the effect of PTX, TQ, PTX-TQ combined nanoparticles on the apoptosis/necrosis assessment in MCF-7 cells after exposure to 24h. Cells were stained with

annexin V-FITC/PI and results were determined using flow cytometry and different cell populations are plotted as a percentage of total events, (b) Graphical representation of apoptosis, necrosis and total cell death. Significance values were compared to control: *$p < 0.05$, **$p < 0.01$, ***$p < 0.001$. All data are shown as the mean ± SD from three independent experiments.

2.9 Cell cycle analysis via flow cytometry

The cell cycle was assessed by staining with propidium iodide to evaluate DNA content following a 48-hour treatment. Untreated MCF-7 cells exhibit a typical asynchronous cycling pattern in the G0/G1 36.66 ± 2.07%, S (32.86 ± 1.22%), G2/M (17.73± 2.08%), and sub-G1 (9.02 ± 1.72%) phases of the cell cycle. The administration of PTX-NPs treatment resulted in a significant accumulation in the G2/M phase (31.70 ± 4.15%) and a reduction in the G0/G1phase (15.72 ± 7.55%), indicative of mitotic checkpoint activation due to microtubule stabilization. TQ- NPs significantly augmented the sub-G1 hypodiploid population (21.17 ± 1.81%) and showed a significant accumulation in S-phase (51.70 ± 0.50%), as shown in Figure 9, suggesting that accelerated apoptotic DNA fragmentation is the primary cellular fate. The PTX-TQ-NPs combination leads more towards apoptosis with accumulation of 34.60 ± 0.55% in the sub-G1 phase. PTX-TQ-Nps also showed the dual perturbation: significant G_2/M accumulation (12.33 ±1.75%]), indicative of PTX's microtubule-stabilizing effect, superimposed by a substantially elevated S fraction (23.53 ± 2.02%), indicative of TQ-NPs behaviour. The simultaneous occurrence of mitotic arrest and advanced apoptotic DNA degradation constitutes a distinctive combinational cell cycle signature, indicating that co-encapsulation facilitates the concurrent operation of PTX-induced mitotic catastrophe and TQ-induced apoptotic priming within the same cellular environment, progressively propelling arrested cells from G2/M into irreversible caspase-mediated disassembly.

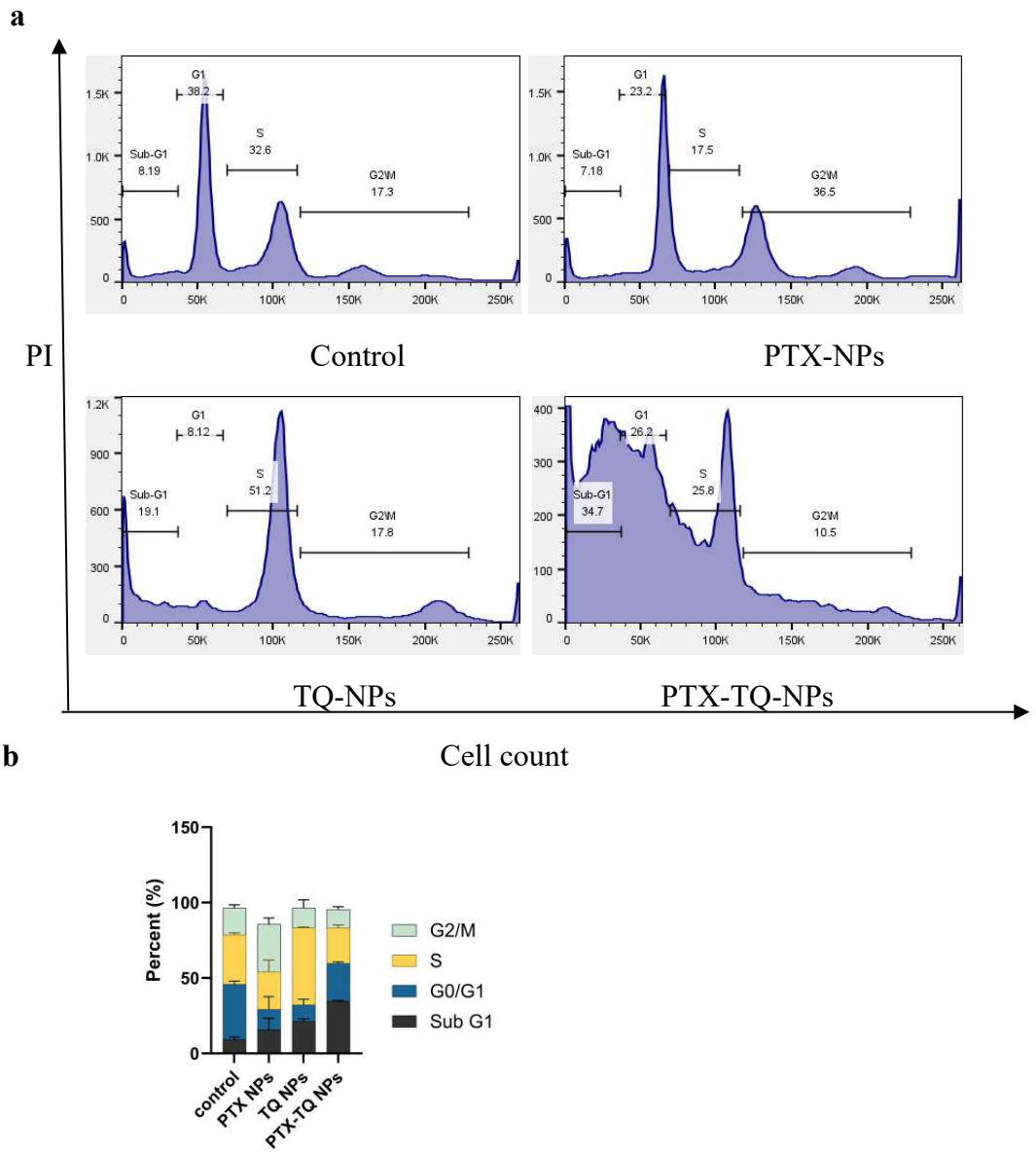
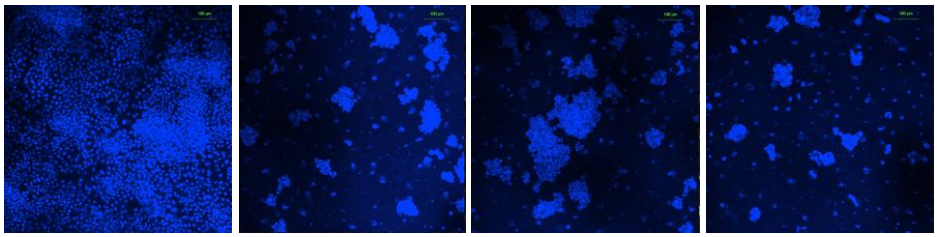


Fig 9 (a) Represents the effect of PTX, TQ, PTX-TQ combined nanoparticles on the cell cycle distribution of MCF-7 cells after exposure to 48 h. Cells were stained with PI and cell cycle distribution was using DNA content flow cytometry analysis and different cell populations are plotted as a percentage of total events, (b) Graphical representation of percentage of Sub G1, G1, S and G2/M phases of the cell cycle. Significance values were compared to control: *$p < 0.05$, **$p < 0.01$, ***$p < 0.001$. All data are shown as the mean ± SD from three independent experiments.

2.10 Nuclear staining using DAPI

To morphologically confirm apoptosis, MCF-7 cells cultured on glass coverslips were treated for 48 h, fixed, permeabilized, and stained with DAPI (Fluoroshield with DAPI), then examined using fluorescence microscopy (λex 360 nm, λem 460 nm). As we can clearly see in Figure 10, untreated control cells, the nuclei exhibited an oval shape, uniform luminescence, and structural integrity, characterized by evenly distributed chromatin and smooth nuclear contours, indicative of viable, actively proliferating cells. Cells treated with PTX- NPs

exhibited early chromatin condensation at the nuclear peripheries, while treatment with TQ-NPs resulted in a moderate irregularity of nuclear chromatin compared to controls. Cells subjected to PTX-TQ-NPs exhibited a comprehensive array of apoptotic nuclear disintegration as well as reduction in the cell number also.



Control PTX-NPs TQ-NPs PTX-TQ-NPs

Fig. 10 represents the effect of PTX-NPs, TQ-NPs, and PTX-TQ-NPs on the nuclear morphology of the MCF-7 cell line.

2.11 Determination of gene expression by quantitative real- time RT-PCR

The transcriptional modulation of the Wnt/β-catenin/TGF-β/EMT regulatory network was analyzed in ten targeted genes (CTNNB1/β-catenin, TGF-β1, CDH1/E-cadherin, CDH2/N-cadherin, VIM/Vimentin, SNAI1/Snail, SNAI2/Slug, Caspase-9, MMP-2, and MMP-9) using the $2^{-}\Delta\Delta Ct$ method, normalized to the housekeeping gene β-actin. The RNA samples from all treatment groups exhibited A260 /A280 ratios ranging from 1.90 to 2.05, indicating acceptable purity for subsequent quantification.

PTX-TQ-NP treatment produced the most extensive transcriptional reprogramming across the entire target panel. CTNNB1 transcript levels were downregulated 0.005 ± 0.01-fold relative to untreated controls, and TGF-β1 mRNA levels were downregulated 0.152 ± 0.01-fold. Among epithelial-mesenchymal transition markers, CDH1 was the only target that showed upregulation 1.49 ± 0.06-fold, indicating transcriptional reactivation of E-cadherin after Snail protein depletion. The mesenchymal repertoire was consistently silenced: VIM was downregulated 0.009 ± 0.01-fold, CDH2 was downregulated 0.034 ± 0.05-fold, and SNAI1, the principal CDH1 transcriptional repressor, was downregulated 0.005 ± 0.01-fold, compared with 1 in untreated controls (Figure 11). This alteration mechanistically predisposes the mitochondrial outer membrane to permeabilization and the initiation of the caspase cascade. The PTX-TQ-NP group showed markedly greater changes than either PTX or TQ nanoparticles alone, indicating synergistic behavior. Gene expression values are shown in Supplementary Table 2.

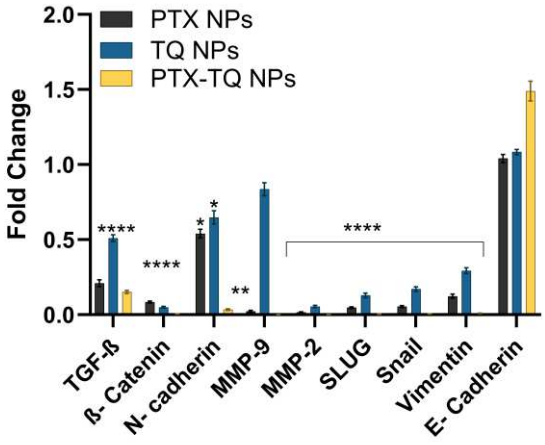


Fig. 11 represents the effect of PTX, TQ, and PTX-TQ combined nanoparticles on different gene expressions of EMT in MCF-7 cells after exposure for 48 h. Total RNA was extracted and subjected to RT-qPCR to measure gene expression. Data were plotted using the $2^{-\Delta\Delta Ct}$ method (expression normalized to the housekeeping gene β-actin). Fold expression and significance were calculated relative to control untreated cells. Significance values were compared to control: *$p < 0.05$, **$p < 0.01$, ***$p < 0.001$. All data are shown as the mean ± SD from three independent experiments.

2.12 Western blot analysis of protein expression related to apoptosis and epithelial-mesenchymal transition (EMT)

2.12.1 Markers of Apoptotic Proteins

Densitometric quantification of immunoblot bands, normalized to β-actin, was employed to evaluate the expression of apoptosis-regulatory proteins. The bands were depicted in Figure 12 (a), and the size of bands was determined by the ImageJ software. In PTX-TQ-NPs-treated cells, the Bax protein exhibited a treatment-dependent increase of 1.78 ± 0.82-fold compared to controls, while Bcl-2 decreased concurrently by 0.65 ± 0.59-fold. The Bax/Bcl-2 protein ratio of 2.74 ± 0.8-fold (compared to controls) mechanistically induces the permeabilization of the outer mitochondrial membrane, leading to cytochrome c release and apoptosome assembly. Thereby confirming the activation of the executioner protease responsible for the final disassembly of cellular structure. The Bax/Bcl-2 ratio was significantly greater in the dual-drug nanoparticle condition compared to all controls as shown in Figure 12 (b), confirming synergistic activation of the intrinsic pathway at the protein level[34].

2.12.2 EMT protein expression and inhibition of the Wnt/β-catenin pathway

A significant decrease in β-catenin protein expression, a key effector and transcriptional co-activator of Wnt signaling-driven EMT, was observed at 0.59 ± 0.07-fold in PTX-TQ-NP-treated cells versus untreated controls, directly confirming suppression of the Wnt/β-catenin pathway at the protein level, as shown in Figure 12 (c). This marked reduction in cytoplasmic and nuclear β-catenin levels mechanistically predicts decreased TCF/LEF-driven transcriptional activation of downstream EMT-driving oncogenes, including cyclin D1, c-Myc,

and matrix metalloproteinases, consistent with Wnt inhibition-mediated EMT reversal observed in various cancer models[35].

The epithelial adhesion protein E-cadherin was strongly up-regulated by 1.55 ± 0.21-fold at the protein level in PTX-TQ-NP-treated cells, confirming RT-qPCR upregulation of CDH1 and indicative of restoration of epithelial junctional integrity. Correspondingly, mesenchymal transition markers N-cadherin (not shown in Figure 12 because no bands appeared after so many repetitions) and Vimentin were reduced by 0.33 ± 0.02. Collectively, these changes at the protein level serve as detailed multi-marker orthogonal validation of the RT-qPCR gene expression data, thereby weaving a coherent mechanistic tale of synergistic induction of apoptosis and complete EMT reversal by PTX-TQ-NP dual-drug nanoparticulate delivery.

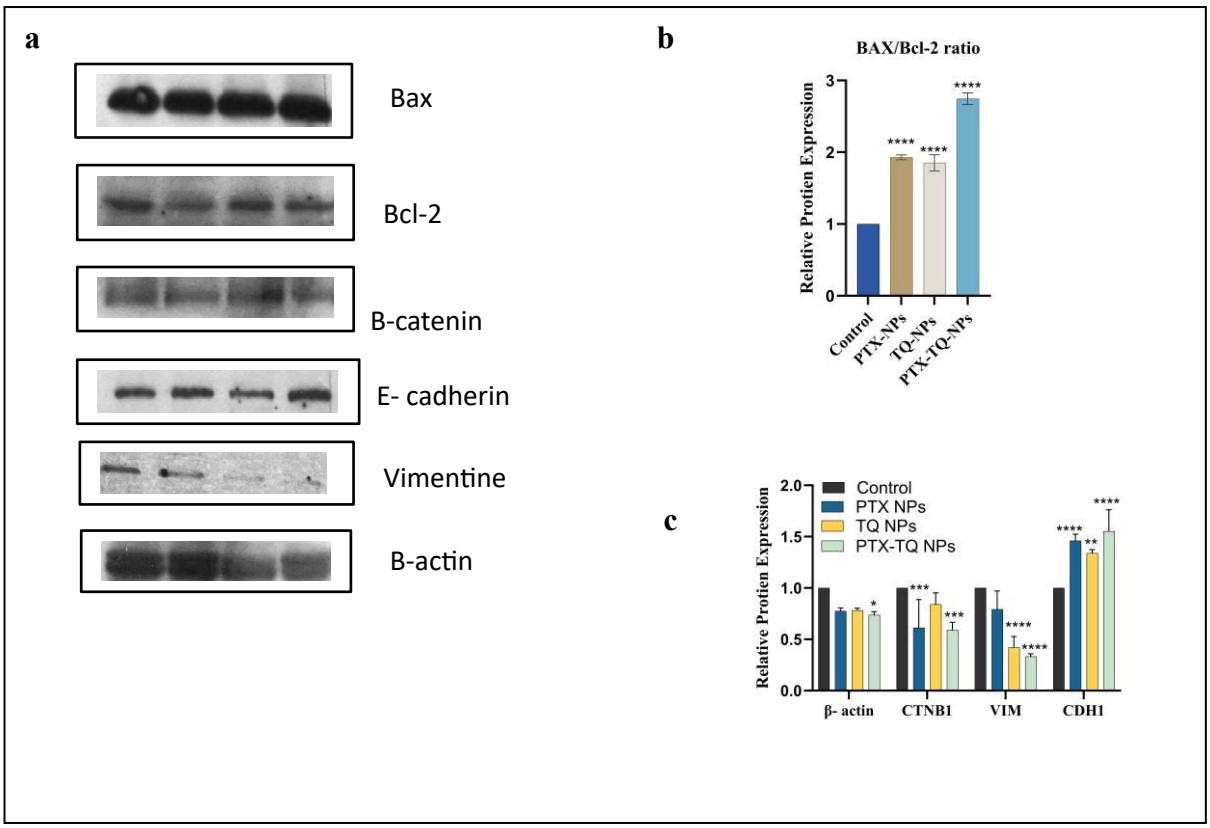


Fig. 12 represents the delineation of the molecular mechanism underlying the anti-migratory effect of the MCF-7 cell line. (a) Western blot analysis depicting the changes in the protein expression levels of Bax, Bcl-2, β-catenin/CTNNB1, E-cadherin/CDH1, and Vimentine/VIM in the treated MCF-7 cell line after 48 h of incubation. β-actin as an internal loading control. (b)The graphical representation of the Bax/Bcl-2 ratio. (c) The graphical representation of differential relative protein expressions of β-catenin/CTNNB1, E-cadherin/CDH1, and Vimentine/VIM in the treated MCF-7 cell line compared to the control. Significance values were compared to the control: *p < 0.05, **p < 0.01, ***p < 0.001. All data are shown as the mean ± SD from three independent experiments.

3 Discussion

The current study demonstrates that co-loading PTX and TQ into Eudragit RS100 nanoparticles produces a synergistic anticancer effect against MCF-7 breast cancer cells. The nanoparticles of PTX, TQ, and PTX-TQ were synthesized successfully using the nanoprecipitation method. The method is popular for its simplicity, reliability, and flexibility. In this method, the polymer solution is combined with water, and the solvent diffuses out rapidly. Rapid mixing of the liquids leads to aggregation of the polymer chains and production of nanoparticles that entrap the hydrophobic pharmaceuticals, without the need of strong shear forces, high temperature, or other harsh conditions, which might destroy the medications or the polymer. The aqueous phase was stabilized using a stabilizer Pluronic F-68 and 0.1% of Tween 80 to avoid aggregation of the freshly produced particles. These stabilizers immediately cover the surface of the particles, keeping them from coming together or growing too big[27,36].

The mean particle size of all the nanoparticles is below 150 nm and the PDI of ~0.2 confirms the narrow, uniform size distribution. The increased size of PTX-TQ nanoparticles in comparison with other nanoparticles is predicted, as the addition of an additional hydrophobic drug improves the internal packing of the polymer core. The size increase is still in the appropriate range for the targeting of the tumor by the enhanced permeability and retention (EPR) effect and does not influence the cellular uptake adversely[28]. In addition, all the nanoparticle compositions showed a positive zeta potential. The aggregation of nanoparticles in the formulation reduces the physical stability of the nanosuspension, whereas nanoparticle aggregation in the gastrointestinal tract results in reduced oral bioavailability. The charge on nanoparticles significantly influences aggregation. A greater quantity of either positive or negative charge repels itself, hence inhibiting aggregation. Generally, suspensions having a zeta potential above ±30 mV are considered physically stable. Suspensions with a zeta potential above ±60 mV demonstrated exceptional stability. Suspensions below around 20 mV have minimal stability, while those below approximately 5 mV experience significant aggregation. All the nanoparticles exhibited the zeta potential in a range of ~25-33 mV, hence are considered physically stable. Zeta potential also affects cellular absorption and therapeutic effectiveness. It is generally known that cationic particles exhibit superior internalization rates compared to their anionic and neutral counterparts, due to the negatively charged nature of the cell membrane[37,38].

The nanoparticles are spherical, as shown by FESEM and TEM images in figure 1. This shape is important because spherical particles have a lower surface area-to-volume ratio. This helps to prevent undesirable medication leaks and allows for a more regulated drug release. Smooth, spherical particles are also less immediately seen and swiftly destroyed by immune cells, which could let them remain in the body longer. TEM images showed a core-shell structure with a darker outer shell consisting of the polymer and a lighter inner core rich in drug. This is the sequence that would be expected from the encapsulation mechanism.

XRD and DSC independently confirmed the loss of crystalline structures of PTX and TQ and their molecular dispersion in Eudragit RS 100 matrix upon formation of the nanoparticles. In XRD, a single broad amorphous halo was observed for all the nanoparticles; fewer sharp peaks were observed. In DSC, the melting peaks of both drugs, clearly visible in the pure materials and were completely missing in the thermogram of the nanoparticles. This transformation from crystalline to amorphous is therapeutically significant as an amorphous drug has a higher energy state than a crystalline drug, which directly translates to better apparent solubility and

faster dissolution - a benefit that is particularly valuable for drugs like PTX and TQ, both of which are poorly water soluble [39].

FTIR confirmed the encapsulation of PTX and TQ without any chemical reaction between the drugs and polymer, which confirmed that all major chemical bonds of PTX and TQ were intact. The slight changes seen in the carbonyl and quinone stretching peaks of TQ and PTX in the nanoparticle spectrum are most likely attributed to non-covalent interactions such as hydrogen bonding, hydrophobic contacts, and probably electrostatic attractions between the positively charged ammonium groups of the polymer and the electronegative oxygen atoms of the drug molecules[26]. These molecular-level interactions help to anchor the drugs in the polymer core and contribute to the sustained, controlled drug release as observed in vitro.

The drug release profile exhibited a two-phase pattern with a rapid initial release in the first 24 hours followed by a slow and sustained release up to 72 h. This behaviour is in accordance with the drug release mechanism of Eudragit RS 100[25]. Such prolonged exposure is therapeutically desirable, as it keeps drug concentrations within tumour cells well above the threshold for anticancer activity for a significant period. This contrasts with free drug solutions that are rapidly cleared and leave cells without drug exposure for significant periods of time.

3.1 Effect of PTX-TQ-NPs on the Apoptosis of Breast Cancer Cells

The combination index (CI) of 0.78, which is less than 1.0, formally demonstrated that PTX and TQ have a synergistic rather than additive effect when co-delivered from the nanoparticles[31]. This synergism is biologically sensible when the mechanisms of the two drugs are placed alongside one another. PTX stabilizes microtubule polymers in the assembled state, preventing MCF-7 cells from completing cell division and trapping them at the G2/M phase of the cell cycle. Such a prolonged arrest leads to stress signals that push the cell towards programmed death by gradually changing the balance of mitochondrial regulatory proteins[40]. TQ acts in a different but complementary way, decreasing the levels of Bcl-2 protein independently, increasing the expression of Bax, and producing reactive oxygen species that damage the mitochondrial membrane, decreasing the threshold at which cells commit to apoptosis[41]. Co-encapsulation ensures that both PTQ and TQ reach the same cell, at the same time, so that their individual pro-apoptotic inputs converge on the same mitochondrial death machinery and produce a combined effect greater than PTX-NPs and TQ-NPs alone. Another benefit of this formulation is that Poloxamer 188 has been reported to inhibit P-glycoprotein (P-gp) efflux pumps. The inhibition of P-gp efflux pumps perhaps decreases the efflux of PTX from the cancer cells and improves the intracellular PTX concentration. [27].

The absence of colony formation in the presence of PTX-TQ-NPs treatment is especially noteworthy since colony assays reflect reproductive potential in the long-term, i.e., the ability of cells that survive early drug exposure to recover and multiply again. This is a more stringent and clinically relevant measure than short-term viability assays, as it is the cells that retain clonogenic potential after chemotherapy that are responsible for tumour relapse. The complete eradication of this surviving fraction by PTX-TQ-NPs, whereas PTX-NPs and TQ-NPs spared significantly more cells, shows the therapeutic depth possible with sustained co-delivery[42].

Flow cytometry showed that 48.41 ± 7.17%, of the cells undergo apoptosis in the presence of PTX-TQ nanoparticles, which was significantly higher than the apoptosis rates induced by either single nanoparticle. The dose ranking was clearly demonstrated in the dot plots with the

shift of the population from viable to early and late apoptotic fractions (Q4, Q3 and Q2), with few necrotic cells, confirming the orderly caspase-mediated cell death rather than non-specific toxic rupture[43].

Cell cycle data added another dimension of understanding. As expected from its microtubule-locking action, PTX-treated cells accumulated mainly in G_2/M. TQ alone arrests the cells at S phase and slightly increases the sub-G1 fraction, which indicates DNA fragmentation that occurs in cells undergoing apoptosis. PTX-TQ-NPs did both at the same time; a unique double pattern not observed with any single nanoparticle treatment. This makes mechanistic sense; PTX arrested cells at mitosis, and TQ's prior reduction of the Bcl-2 safety threshold meant that a shorter period of mitotic arrest was sufficient to tip cells into apoptotic exit rather than abnormal division[44].

DAPI stained nuclei obtained from cells treated with PTX-TQ-NPs exhibited all the classical visual aspects of this process observed under the fluorescence microscope, including condensed, brightly staining chromatin, nuclear lobes in a fragmented state, and well-formed apoptotic bodies[45].

The mechanical explanation was supported by Western blot data: The Bax protein was upregulaed, Bcl-2 protein was downregulated, and the Bax/Bcl-2 ratio was significantly increased in cells treated with the combined nanoparticles as well as in individual nanoparticles also. When Bax is dominant, it perforates the outer mitochondrial membrane and releases cytochrome c into the cytoplasm, where it triggers the apoptosome complex and activates caspase-9, which in turn cleaves and activates caspase-3[33].

3.2 Effect of Combined PTX-TQ-NPs on the EMT of Breast Cancer Cells

Cancer cells transform from an organized, stable epithelial state to a loosely attached, migratory mesenchymal state – a process called epithelial-mesenchymal transition (EMT), to acquire the ability to migrate and invade surrounding tissue. This change in breast cancer is largely driven by the Wnt/β-catenin signalling pathway: when Wnt signalling is active, β-catenin accumulates in the nucleus and activates genes that encourage the mesenchymal phenotype, including those that make matrix metalloproteinases (MMPs) that degrade the surrounding tissue barrier, and N-cadherin, an adhesion protein that facilitates cellular detachment and migration[19] as shown in figure 13. TGF-β1 promotes this process through a separate but interconnected signalling pathway. The two pathways reinforce each other through autocrine feedback loops, making the mesenchymal state self-sustaining once initiated[46].

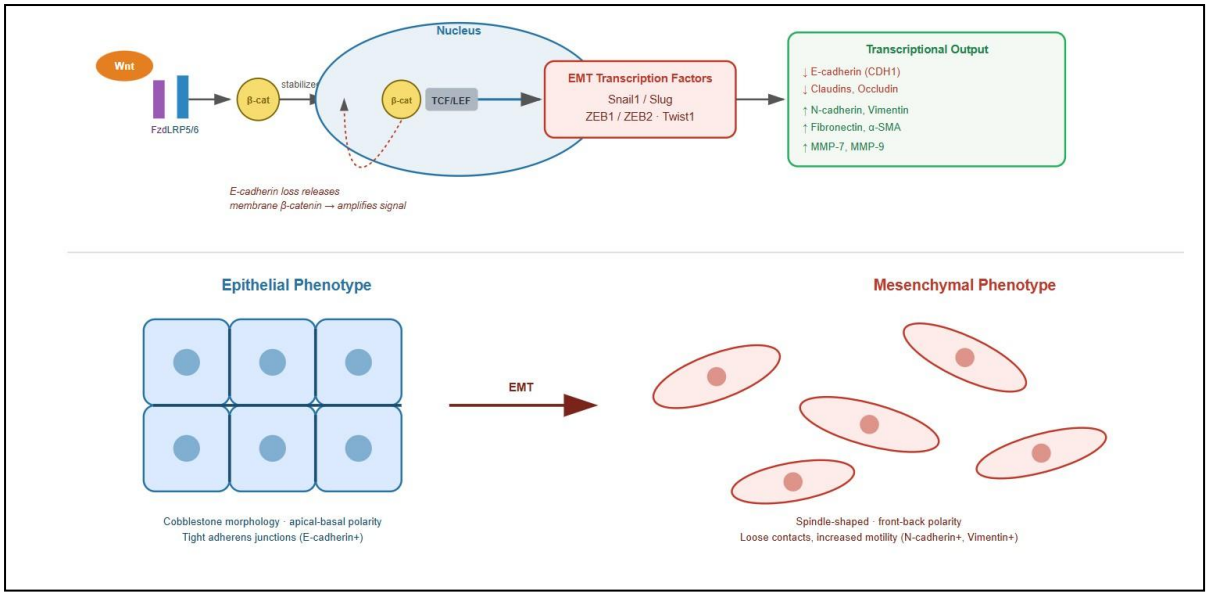


Fig. 13 shows that activation of the canonical Wnt/β-catenin signaling pathway promotes the epithelial-to-mesenchymal transition (EMT). Binding of Wnt ligands to the Frizzled/LRP5/6 receptor complex inhibits β-catenin degradation, enabling its cytoplasmic accumulation and nuclear translocation. Nuclear β-catenin associates with TCF/LEF transcription factors to induce EMT-related transcriptional regulators like Snail and Slug. These factors repress the epithelial junction proteins (E-cadherin, claudins, occluding) and upregulate the mesenchymal markers (N-cadherin, vimentin, fibronectin) as well as matrix-metalloproteinases (MMP-9, MMP-7). The resulting molecular reprogramming drives the transition from a cobblestone-like epithelial phenotype with strong cell- cell adhesion to a spindle-shaped mesenchymal phenotype characterized by reduced intercellular contacts, enhanced motility, and invasive behaviour. This figure was made in MS Power Point.

PTX-TQ-Eudragit-NPs interrupted this cycle at several points. Both β-catenin RNA and protein are down-regulated, removing the upstream Wnt transcriptional drive. Less β-catenin in the nucleus meant less activity of MMP genes, which meant the proteolytic machinery of cancer cells needed to cleave through the extracellular matrix was gone. That's why migration through the transwell dropped off sharply in the transwell assay. Additionally, N-cadherin was downregulated ~0.34-fold, and E-cadherin was upregulated 1.5-fold, reversing the cadherin switch, one of the earliest and most characteristic features of EMT [20,47]. E-cadherin restoration is important for reasons beyond being an obvious marker: E-cadherin molecules physically connect neighbouring cells and anchor cytoplasmic β-catenin to the cell membrane rather than allowing it to enter the nucleus, creating a reinforcing loop that stabilizes the epithelial state[48].

PTX-TQ-NPs treatment also significantly downregulated TGF-β1 transcript levels to disrupt the second arm of the autocrine EMT-sustaining circuit. Vimentin, an intermediate filament protein, was also downregulated. Upregulation of vimentin provides mesenchymal cells with the mechanical flexibility they need to squeeze through tight spaces during invasion; therefore, the reduction of vimentin would physically impair the cytoskeletal remodelling required for directional cell movement[49]. Together, these molecular changes explain the ~90% decrease in wound closure and dramatic abrogation of transwell migration: the cells just lost the

molecular tools to move and penetrate tissue barriers. The combination nanoparticles induced greater changes in all the markers than any single drug treatment, consistent with the pharmacological synergism observed in the CI analysis.

4 Materials and Methods

4.1Materials

Paclitaxel (PTX, purity ≥98%) and Thymoquinone (TQ, purity ≥98%) were purchased from Sigma-Aldrich, India. Polymer used for nanoparticle preparation [Eudragit RS 100((ethyl acrylate-co-methyl methacrylate-co trimethyl ammonium ethyl methacrylate chloride) (1:2:0.1), Pluronic F-68, plant tissue culture tested, Dulbecco's Modified Eagle's Medium (DMEM), penicillin-streptomycin, phosphate-buffered saline (PBS, pH 7.4), trypsin-EDTA, MTT [3-(4,5-dimethylthiazol-2-yl)-2,5-diphenyltetrazolium bromide were purchased from Hi-media, India. Dimethyl sulfoxide (DMSO) and acetone (HPLC grade) were purchased from SRL, India. Fetal bovine serum (FBS) was obtained from Gibco (Thermo Fisher Scientific, India). DAPI (Mounting medium, Fluoroshield with DAPI) reagent was purchased from Sigma-Aldrich. Annexin V-FITC/Propidium Iodide (PI) Apoptosis Detection Kit was bought from Thermofisher, India. RNA isolation kit and cDNA synthesis kits were purchased from Thermo Fisher Scientific, India. The primary antibodies against Bax, Bcl-2, CDH2, β-catenin/CTNNB1, E-cadherin/CDH1, Vimentine/VIM were purchased from Invitrogen (Invitrogen by thermofisher, India), and respective secondary antibody conjugated to the enzyme HRP (Horseradish peroxidase) were also purchased from Invitrogen.

4.2 Maintenance of Cell Line

The human breast adenocarcinoma MCF-7 cell lines used in this study were obtained as a generous gift from the National Institute of Immunology (NII), New Delhi. MCF-7 cells were cultured in DMEM media supplemented with 10% fetal bovine serum (FBS), penicillin (100 U/ml), and streptomycin (100 µg/ml) and kept at 37 ^{0}C in a humidified 5% CO_2 atmosphere.

4.3 Preparation of Nanoparticles

The nanoprecipitation method was used to prepare nanoparticles of Paclitaxel and Thymoquinone individually and in combination with slight modification [50]. In brief, the organic phase was prepared by dissolving Paclitaxel, Thymoquinone, and Eudragit RS 100 in acetone (HPLC grade) with a ratio of 0.5:0.5:10 and a total concentration of 1.25 mg/ml of PTX and TQ, and 12.5 mg/ml of polymer under sonication in an ultrasonic bath sonicator (ultrasonic bath, Emerson, USA) at high frequency (40 KHz) for an hour. The aqueous phase was prepared by dissolving Pluronic F-68 (concentration 5 mg/ml) and 0.1 percent of Tween 80 as a surfactant in deionized water. After sonication, the organic phase was added dropwise at a constant flow rate into the aqueous phase with constant stirring using a magnetic stirrer at 1000 rpm. Gradually, the solution turned turbid, indicating the preparation of nanoparticles. The stirring process was continued overnight on the magnetic stirrer for the evaporation of organic solvent, i.e., acetone, at room temperature, after which the solution was centrifuged at 3000 RPM for 10 minutes to remove free TQ. Further, the nanoparticles were characterized to determine their size. Paclitaxel and thymoquinone nanoparticles were also prepared similarly by keeping the ratio same as 1:10 of drug to polymer. Blank nanoparticles were also prepared following the same procedure without adding Paclitaxel and Thymoquinone.

4.4 Physiochemical Characterization of Nanoparticles

4.4.1 Particle size, Poly Dispersity Index, and Zeta- potential:

The size, size distribution (Poly Dispersity Index), and zeta- potential of PTX, TQ, and PTX-TQ nanoparticles were measured by the dynamic light scattering (DLS) method using Zetasizer (Malvern Instrument, Malvern UK). The results were presented as means ± standard deviation, based on three independent measurements.

4.4.2 Size and Shape of Nanoparticles

A Field Emission Scanning Electron Microscopy (FESEM) and Transmission Electron Microscopy (TEM) were used to observe the morphology, shape, and size of nanoparticles. For FESEM, before the imaging process, the nanoparticles were coated with a layer of gold using an Auto Fine Coater. For TEM, a drop of nanoparticles was placed on a copper grid with a mesh size of 300. A drop of phosphotungstic acid was added and left for 10 seconds. The films were air-dried for 5-10 minutes and observed under a microscope. The samples were analysed at 60–80 KV at a resolution of 1550Å.

4.4.3 Differential Scanning Calorimetric (DSC):

DSC was carried out to measure how the physical properties of a sample change, along with temperature, over time. 5 mg of each lyophilized sample of PTX and TQ and PTX-TQ NPs were placed in an aluminium pan, which was sealed tightly and heated in a range from 25 ^{0}C to 400 ^{0}C with a heating rate of 10 ^{0}C/min, with nitrogen acting as a purge gas to regulate the system's temperature.

4.4.3 Fourier transform infrared FTIR:

FTIR spectra of PTX, TQ, and PTX-TQ NPs were determined by using a Cary 600 series FTIR spectrometer (Agilent Technologies, USA) to validate the quality of synthesis, including drug entrapment in nanoparticles and assessment of conjugation. In brief, a pellet was formed by taking a small amount (approx. 1 mg) of nanoparticles mixed with spectroscopic grade potassium bromide (approx. 10 mg). FTIR spectroscopy was conducted by scanning nanoparticles for absorbance through a range of 4 to 4000 cm^{-1} wavenumbers at a resolution of 1 cm^{-1}.

4.4.4 X-ray Diffraction

The X-ray diffraction (XRD) patterns of PTX, TQ, and PTX-TQ NPs were examined using Advanced X-ray Diffractometer. The samples were analysed within an angle of 2θ range of 10° to 90° at a scanning rate of 4°/min.

4.5 The Entrapment Efficiency

The synthesized nanoparticles were assessed for encapsulation efficiency by calculating PTX and TQ in the supernatant of their respective NPs and in combined NPs. The synthesized NPs were dissolved in methanol and centrifuged at 10,000 rpm for 30 min at 4°C, and the supernatant was collected. The unentrapped PTX and TQ were diluted further and quantified using a UV spectrophotometer at 228 and 254 nm, respectively. The amount of PTX and TQ was estimated from the standard curve of PTX and TQ in methanol, respectively. The Entrapment Efficiency % and Drug Loading % were determined using the following equation 1 and 2[51]

$$EF\% = \frac{Total\ amount\ of\ drug - Amount\ of\ free\ drug}{Toatl\ amounnt\ of\ drug} \times 100 \quad (1)$$

$$DL\ \% = \frac{Drug\ Loaded}{Toatal\ weight\ of\ NPs} \times 100 \quad (2)$$

4.6 In vitro release study

In-vitro drug release study was performed by the dialysis membrane diffusion method. In brief, 5 mg of each nanoparticle was dispersed individually in 5 ml of phosphate buffer at pH 7.4 and placed into a dialysis membrane-70 (Hi media, India). The membrane was activated overnight before use. The membrane was immersed in 100 ml of the corresponding phosphate buffer in a glass beaker and stirred at 150 rpm and at 37°C. Aliquots of 3 mL of the release medium were withdrawn at time intervals of 0, 1, 2, 4, 8, 12, 24, 48, and 72 h and replaced with an equal volume of fresh PBS to maintain sink conditions. The drug concentrations in the collected aliquots were determined by UV-vis spectroscopy, and the absorbance was measured at 228 nm and 254 nm to quantify the release of PTX and TQ from NPs, respectively. The release studies of free PTX and free TQ were also carried out using the same protocol. Cumulative drug release (%) was determined and plotted against time. The release data were fitted to zero-order, first-order, Higuchi, and Korsmeyer-Peppas kinetic models to elucidate the mechanism of drug release[52].

4.7 Cell viability assay

The cytotoxicity of free PTX, free TQ, combined free PTX-TQ, blank NPs, PTX- NPs, TQ-NPs, and combined PTX-TQ NPs on the MCF-7 cells was evaluated by MTT colorimetric assay. To find out the synergistic behaviour of PTX and TQ nanoparticles, individual NPs of both were used in combination. For this study, cells were taken out of the tissue culture flask after trypsinization, and a single-cell suspension was made. 3×10^4 cells/well were seeded into 96-well plates and incubated for 24 hr for adhesion. After adhesion, cells were treated with serial dilution of each formulation (concentration range for free PTX and PTX-NPs [0.001-5 µg/ml], for free TQ, TQ- NPs and blank NPs [1- 40 µg/ml], for PTX-TQ-NPs [0.5-20 µg/ml], and for free PTX- TQ and PTX- TQ NPs [0.001-5 µg/ml of PTX and fix concentration of 4 µg/ml of TQ] for 24, 48, and 72 hr. At each time point, 20 µl of MTT solution (5 mg/mL in PBS pH 7.0) was added to each well and incubated for 3 hr at 37 ^{0}C. After 3 hours of incubation, the formed formazan crystals were dissolved in 200 µl of DMSO, and the absorbance was measured at 570 nm using a microplate reader (Thermo Scientific Multiskan FC microplate reader). Cell viability is presented as % compared with untreated control cells. The MCF-7 cells were treated with PTX-NP and F-PTX in combination with a fixed concentration of TQ-NPs and F-TQ, respectively, to calculate the synergistic effect of both treatments. The half-maximal inhibitory concentration (IC_{50}) was calculated with GraphPad Prism (v 10.0) using nonlinear regression. Free PTX and free TQ were dissolved in DMSO. The concentration of DMSO was less than 0.1%.

4.8 Colony assay

A colony assay was performed to evaluate the impact of nanoparticles on the MCF-7 cell line. 500 cells per well were seeded into a 12-well plate and incubated for 24 hours for adhesion. After 24 hr cells were treated with the predetermined IC_{50} values and at values lower than the IC_{50} of the nanoparticles for 14 days at 37 ^{0}C. Every 3rd day, the media was replaced with fresh media. After incubation, colonies were rinsed twice with 1x PBS and fixed with 10% methanol

for 15 minutes. After fixation, the colonies were rinsed twice with 1x PBS and stained with 0.1% crystal violet solution (Gram's crystal violet) for 10 minutes. Then again, the plates were washed twice with PBS, and colonies were counted[53].

4.9 Wound healing assay

A wound healing assay was used to evaluate cell migration. MCF- 7 cells at a cell density of 3×10^4 cells/well were grown in a 24-well plate. The next day, a scratch was made in the centre of the well using a sterile 200 µl pipette tip to generate a linear wound. After scratching, the cells were washed twice with PBS to remove the detached cells, and fresh DMEM containing the treatment formulation was added. To assess the migration rate, cells were treated with predetermined IC_{50} and concentrations below IC_{50}. Images of the scratch were taken at 0, 24, and 48 hr. The area of wound closure was measured using ImageJ software (ImageJ Java1.8.0) and expressed as a percentage of the initial scratch area. Migration rate (%) was determined by the following formula:

$$Migration\ rate\ (\%) = \frac{(Wound\ Area\ at\ 0\ h - Wound\ Area\ at\ t\ h)}{Wound\ Area\ at\ 0\ h} \times 100$$

4.10 Transwell Migration Assay Assay

The transwell migration assay was carried out using cell culture inserts **(**Corning Transwell 6-well plates) with an 8 µm pore size. Culture inserts were set up in a 6-well plate. In the top chamber, MCF-7 cells with a cell density of 1×10^6 /well were placed in serum free DMEM media with the respective treatment. In the lower chamber, 1ml of DMEM media with 10% FBS was added and incubated for 24 h and 48 hr. FBS acts as a chemoattractant for cells. After the incubation of 24 and 48 hours, the cells in the inserts were washed with PBS, fixed with 4% paraformaldehyde, and permeabilized with methanol. Furthermore, the cells were stained with crystal violet dye for 30 minutes. The cells located in the bottom section of the inserts were counted under a light microscope. Five random fields per insert were imaged, and the mean number of migrated cells per field was determined. Migration rate was determined by the following formula:

$$Migration\ rate\ (\%) = \frac{Migrated\ cells\ in\ treated\ group}{Migrated\ cells\ in\ control\ group} \times 100$$

4.11 Analysis of cell apoptosis by Flow Cytometry

Cell apoptosis and necrosis were assessed by flow cytometry analysis using an Annexin V-FITC/ PI double staining apoptosis detection kit (Sigma-Aldrich). The MCF- 7 cells were seeded at 1×10^6 /well and were treated with PTX NPs, TQ NPs, and PTX-TQ NPs at predetermined IC_{50} concentrations for 48 hr. Simultaneously, a control group of untreated cells was also cultured. For every treated and control group, three replicates were considered. Following the manufacturer's instructions, cells were trypsinized, washed twice with PBS, and resuspended in 1x Annexin V binding buffer at a density1×10^6 cell/ml. The cells were then incubated with 5 µl of Annexin V-FITC and 10 ul of PI solution and incubated for 10 minutes at room temperature in the dark. Flow cytometry analysis was conducted on a BD FACSDiva 9.0.1 (BD Biosciences, USA), and at least 50000 events were collected per sample. The FL1

and FL2 signal detectors (λex/em 488/530 nm for FITC and λex/em 535/617 nm for PI) were then used to evaluate the fluorescence signals. Data were analyzed using FlowJo software (FlowJo 10.10.0). Cells were classified as viable (Annexin V−/PI−), early apoptotic (Annexin V+/PI−), late apoptotic (Annexin V+/PI+), and necrotic (Annexin V−/PI+). The total apoptosis was calculated as the sum of early and late apoptotic populations.

4.12 Analysis of cell cycle by Flow Cytometry

To examine the impact of NPs on cell cycle distribution, MCF-7 cells were treated with predetermined IC_{50} values of PTX, TQ, and PTX-TQ-NPs for 48 hr. A control group of untreated cells was also cultured simultaneously. After treatment, cells were trypsinized, harvested, rinsed with ice-cold PBS, and resuspended in 500 µl of PBS. To secure cell fixation, 1ml of 70 % ethanol was added to cells during vortexing. Cells were incubated at 4 ^{0}C for 1 hr. Before analysis, cells were washed and resuspended in 1ml of PBS containing 50 µg/ml RNAase A and 10 µg/ml propidium iodide (PI). Cells were cultured in the dark at 37^{0}C for 20 minutes and then examined for DNA content using flow cytometry with FL 2 signal detector λex/em 535/617 nm.

4.13 Nuclear staining using DAPI

To assess the morphology of nuclear DNA of cells, the cells were treated with DAPI. In a 6-well plate, glass coverslips were placed, and MCF-7 cells were seeded with a cell density of 1×10^6 /well. The cells were allowed to adhere to the glass coverslip for 24 hours. After 24 hours, the cells were treated with predetermined IC_{50} values of PTX, TQ, and PTX-TQ-NPs. After 48 hours of incubation, the cells were washed with PBS and fixed with 4 % paraformaldehyde solution for 15- 20 minutes. After fixation, cells were permeabilized with methanol and treated with DAPI mounting medium (2-3 drops) and incubated at room temperature for 30 minutes in a dark room, then visualized under a Nikon confocal laser scanning microscope at 20x.

4.14 EMT gene expression analysis

Real-time polymerase chain reaction (RT-PCR) was conducted to evaluate the expression levels of EMT genes. The total RNA was extracted from the cells after 48 h of treatment with PTX, TQ, and PTX-TQ NPs at predetermined IC_{50} values using an RNA isolation kit (PureLink RNA Mini Kit, Invitrogen) according to the manufacturer's instructions. The RNA and its purity were verified (A260/280>1.9-2.15) with a Nanodrop Spectrophotometer (NANODROP 2000, Thermo Scientific). Thereafter, 1 µg of the total RNA was reverse transcribed to create a cDNA library using a cDNA synthesis kit (Verso cDNA synthesis kit, Thermofisher, India), with random hexamers in a 20 µl reaction. The cDNA was then subjected to quantitative real-time PCR using a master mix (2X QuantiNova SYBRGreen Master Mix). PCR cycling conditions were 5 min at 94°C for initial denaturation, followed by 40 cycles of 15 s at 94°C for denaturation and 30 s at 58°C for annealing/extension and melting at 66°C to 99 C for 90 s. β-actin served as a housekeeping gene; normalized fold changes for all target genes were calculated using the formula: $2^{-(\Delta\Delta Cq)}$[54] The expression of the following targeted genes was analysed: β-catenin (CTNNB1), TGF-β1, E-cadherin (CDH1), N-cadherin (CDH2), Vimentin (VIM), Snail (SNAI1), Slug (SNAI2), MMP-2, MMP-9. The sequences of the primers were designed using Primer3 software and are provided in Supplementary Table S2.

4.15 Western Blot Analysis

The protein expression levels of key apoptotic and EMT-related markers, including E-cadherin, N-cadherin, Vimentin, Bcl-2, and Bax, were evaluated by western blot analysis. MCF-7 cells were treated and then lysed on ice for 30 min in RIPA buffer (Sigma- Aldrich, India) containing protease and phosphatase inhibitor cocktails (Complete™, Mini, EDTA-free Protease Inhibitor Cocktail, Merck, India). Lysates were centrifuged at 13,200 rpm for 20 min at 4°C. Protein concentration was determined by the Bradford assay. Equal amounts of protein (30 µg) were separated by SDS-PAGE on 10% polyacrylamide gels and transferred to a nitrocellulose membrane (0.45 µm, Hi-Media), using a wet transfer system. Membranes were blocked for 1 h at room temperature with 3% skimmed milk in Tris-buffered saline with 0.1% Tween-20 (TBST) and incubated overnight at 4 °C with the appropriate primary antibodies (dilutions as per manufacturer's instructions). Membranes were washed three times for 5 minutes with TBST and then incubated with the appropriate secondary antibodies conjugated to HRP (Horseradish peroxidase), using a dilution of 1:15000 with TBST for 1 h at room temperature. Protein bands were detected by an enhanced chemiluminescence (ECL) system and visualized by X-ray film in a dark room. Band densities were quantified with ImageJ software and normalized to β-actin as a loading control.

5 Conclusion

The PTX, TQ, and PTX-TQ co-loaded polymeric nanoparticles were successfully synthesized by the nanoprecipitation method, and promising physicochemical properties such as nanoscale size, narrow size distribution, suitable surface charge, high encapsulation efficiency, and sustained biphasic drug release were observed. The amorphous nature of the nanoparticles was confirmed by XRD and DSC analyses, whereas the FTIR analysis indicated the physicochemical compatibility between the drug and the polymer. The biological evaluation in MCF-7 breast cancer cells showed a synergistic antiproliferative activity (CI<1), significant clonogenic inhibition, blockage of cell migration, induction of intrinsic apoptosis, concurrent G2/M phase and sub-G1 accumulation arrest, as well as morphological apoptotic nuclear fragmentation confirmed by DAPI. RT-qPCR and Western blot analyses showed a wide-ranging, comprehensive suppression of the Wnt/β-catenin/EMT pathway, as demonstrated by the downregulation of β-catenin, TGF-β, Snail, N-cadherin, and Vimentin, and the upregulation of E-cadherin, thus providing a physiologically adequate rationale for the observed anti-migratory and anti-invasive effects. The accumulating results provide thorough in vitro validation for breast cancer treatment, shown by an increased Bax/Bcl-2 ratio.

Statistical Analysis

All experiments were performed in triplicate and repeated at least three times independently. Data are presented as mean ± standard deviation (SD). Statistical comparisons between groups were performed using two-way analysis of variance (ANOVA) followed by Tukey's post-hoc test for multiple group comparisons, using GraphPad Prism software (version 10.0, GraphPad Software, San Diego, CA, USA). A p-value of less than 0.05 ($p < 0.05$) was considered statistically significant. Combination index (CI) values for drug synergy were calculated using the Chou-Talalay method via CompuSyn software (ComboSyn Inc., NJ, USA), where $CI < 1$, $CI = 1$, and $CI > 1$ indicate synergism, additivity, and antagonism, respectively.

Acknowledgement

We thank Dr. Anil Kumar, National Institutes of Immunology, New Delhi, for providing the MCF-7 breast cancer cell line.

Authors contribution

R.S. performed the experiments, data preprocessing, analysis, visualization, and drafted the manuscript. M.K. contributed to methodology development and assisted in data interpretation. M.V. supported validation and manuscript editing. R.B contributed to computational analysis and software implementation and also provided lab space. N.S. conceptualized and supervised the study, guided interpretation, and finalized the manuscript

Data Availability Statement

The authors confirm that the data supporting the findings of this study are available within the article [and/or] its supplementary materials.

Funding: This work was supported by the Department of Health Research, Ministry of Health and Family Welfare (GOI). The grant number is R-12013/17/2020-HR.

Clinical trial number: Not applicable.

Discloser Statement: The authors declare no conflicts of interest and that no ethical clearance is required.

Abbreviations

PTX- Paclitaxel
TQ- Thymoquinone
NPs- Nanoparticles
EMT- Epithelial-to-Mesenchymal Transition

References

[1] Mubarik S, Wang F, Nadeem AA, Fawad M, Yu C. Breast cancer epidemiology and sociodemographic differences in BRICS-plus countries from 1990 to 2019: An age period cohort analysis. SSM Popul Health 2023;22. https://doi.org/10.1016/j.ssmph.2023.101418.

[2] Eleotério MR, Ferreira LS, Azevedo FM, Candido AC, Franceschini S do CC, de Souza ECG. Folate Intake and Breast Cancer Risk: A Systematic Review and Meta-Analysis. Mol Nutr Food Res 2026;70. https://doi.org/10.1002/mnfr.70354.

[3] Motiwala MN, Rangari VD. Combined effect of paclitaxel and piperine on a MCF-7 breast cancer cell line in vitro: Evidence of a synergistic interaction. Synergy 2015;2:1–6. https://doi.org/10.1016/J.SYNRES.2015.04.001.

[4] Peng J, Fumoto S, Miyamoto H, Chen Y, Kuroda N, Nishida K. One-step formation of lipid-polyacrylic acid-calcium carbonate nanoparticles for co-delivery of doxorubicin and curcumin. J Drug Target 2017;25:704–14. https://doi.org/10.1080/1061186X.2017.1315687.

[5] Solak K, Yildiz Arslan S, Acar M, Turhan F, Unver Y, Mavi A. Combination of magnetic hyperthermia and gene therapy for breast cancer. Apoptosis 2025;30:99–116. https://doi.org/10.1007/s10495-024-02026-4.

[6] Abouzeid AH, Patel NR, Torchilin VP. Polyethylene glycol-phosphatidylethanolamine (PEG-PE)/vitamin e micelles for co-delivery of paclitaxel and curcumin to overcome multi-drug resistance in ovarian cancer. Int J Pharm 2014;464:178–84. https://doi.org/10.1016/j.ijpharm.2014.01.009.

[7] Zhao S, Tang Y, Wang R, Najafi M. Mechanisms of cancer cell death induction by paclitaxel: an updated review. Apoptosis 2022;27:647–67. https://doi.org/10.1007/s10495-022-01750-z.

[8] Medhi H, Khumukcham SS, Manavathi B, Paik P. Effective: In vitro delivery of paclitaxel by nanocargo of mesoporous polycaprolactone against triple negative breast cancer cells by minimalizing drug dose. RSC Adv 2020;10:24095–107. https://doi.org/10.1039/d0ra04505e.

[9] Dong X, Mattingly CA, Tseng M, Cho M, Adams VR, Mumper RJ. Development of new lipid-based paclitaxel nanoparticles using sequential simplex optimization. European Journal of Pharmaceutics and Biopharmaceutics 2009;72:9–17. https://doi.org/10.1016/j.ejpb.2008.11.012.

[10] Zhong Y, Su T, Shi Q, Feng Y, Tao Z, Huang Q, et al. Co-administration of irgd enhances tumor-targeted delivery and anti-tumor effects of paclitaxel-loaded plga nanoparticles for colorectal cancer treatment. Int J Nanomedicine 2019;14:8543–60. https://doi.org/10.2147/IJN.S219820.

[11] Xiong K, Zhang Y, Wen Q, Luo J, Lu Y, Wu ZX, et al. Co-delivery of paclitaxel and curcumin by biodegradable polymeric nanoparticles for breast cancer chemotherapy. Int J Pharm 2020;589. https://doi.org/10.1016/j.ijpharm.2020.119875.

[12] Liu M, Fu M, Yang X, Jia G, Shi X, Ji J, et al. Paclitaxel and quercetin co-loaded functional mesoporous silica nanoparticles overcoming multidrug resistance in breast cancer. Colloids Surf B Biointerfaces 2020;196. https://doi.org/10.1016/j.colsurfb.2020.111284.

[13] Ballout F, Habli Z, Rahal ON, Fatfat M, Muhtasib H-G. Thymoquinone-based nanotechnology for cancer therapy: promises and challenges. Drug Discov Today 2018;00. https://doi.org/10.1016/j.

[14] Wang S, Deng H, Wang Y, Rui W, Zhao P, Yong Q, et al. Antimicrobial Activity and Action Mechanism of Thymoquinone against Bacillus cereus and Its Spores 2021.

[15] Samarghandian S, Farkhondeh T, Samini F. A Review on Possible Therapeutic Effect of Nigella sativa and Thymoquinone in Neurodegenerative Diseases. CNS Neurol Disord Drug Targets 2018;17:412–20. https://doi.org/10.2174/1871527317666180702101455.

[16] Bhattacharya S, Ahir M, Patra P, Mukherjee S, Ghosh S, Mazumdar M, et al. PEGylated-thymoquinone-nanoparticle mediated retardation of breast cancer cell migration by deregulation of cytoskeletal actin polymerization through miR-34a. Biomaterials 2015;51:91–107. https://doi.org/10.1016/j.biomaterials.2015.01.007.

[17] Bashmail HA, Alamoudi AA, Noorwali A, Hegazy GA, AJabnoor G, Choudhry H, et al. Thymoquinone synergizes gemcitabine anti-breast cancer activity via modulating its apoptotic and autophagic activities. Sci Rep 2018;8. https://doi.org/10.1038/s41598-018-30046-z.

[18] Neevedha K, Anitha E, Gokul T, Anandan I, Vivekkumar SP. Comparison of Anticancer Activity Between Thymoquinone and Tamoxifen, Thymoquinone + Tamoxifen 0n Mcf-7 Cell Line of Human Breast Cancer –An Invitro Study. Biomedical and Pharmacology Journal 2024;17:1329–34. https://doi.org/10.13005/bpj/2946.

[19] Thiery JP, Acloque H, Huang RYJ, Nieto MA. Epithelial-Mesenchymal Transitions in Development and Disease. Cell 2009;139:871–90. https://doi.org/10.1016/j.cell.2009.11.007.

[20] MacDonald BT, Tamai K, He X. Wnt/β-Catenin Signaling: Components, Mechanisms, and Diseases. Dev Cell 2009;17:9–26. https://doi.org/10.1016/j.devcel.2009.06.016.

[21] Ma F, Li W, Liu C, Li W, Yu H, Lei B, et al. MiR-23a promotes TGF-β1-induced EMT and tumor metastasis in breast cancer cells by directly targeting CDH1 and activating Wnt/β-catenin signaling. 2017.

[22] Lin Z, Wu J, Liu H. Anoikis in cancer: molecular mechanisms, resistance, and therapeutic strategies. Apoptosis 2026;31:192. https://doi.org/10.1007/s10495-026-02402-2.

[23] Zhong Y, Su T, Shi Q, Feng Y, Tao Z, Huang Q, et al. Co-administration of irgd enhances tumor-targeted delivery and anti-tumor effects of paclitaxel-loaded plga nanoparticles for colorectal cancer treatment. Int J Nanomedicine 2019;14:8543–60. https://doi.org/10.2147/IJN.S219820.

[24] Eltaib L. Polymeric Nanoparticles in Targeted Drug Delivery: Unveiling the Impact of Polymer Characterization and Fabrication. Polymers (Basel) 2025;17. https://doi.org/10.3390/polym17070833.

[25] Mostafa MAH, Khojah HMJ. Nanoparticle-based delivery systems for phytochemicals in cancer therapy: molecular mechanisms, clinical evidence, and emerging trends. Drug Dev Ind Pharm 2025;51:1105–21. https://doi.org/10.1080/03639045.2025.2483425.

[26] Thakral S, Thakral NK, Majumdar DK. Eudragit®: A technology evaluation. Expert Opin Drug Deliv 2013;10:131–49. https://doi.org/10.1517/17425247.2013.736962.

[27] Kriplani P, Guarve K. Eudragit, a Nifty Polymer for Anticancer Preparations: A Patent Review. Recent Pat Anticancer Drug Discov 2022;17:92–101. https://doi.org/10.2174/1574892816666211013113841.

[28] Batrakova E V., Kabanov A V. Pluronic block copolymers: Evolution of drug delivery concept from inert nanocarriers to biological response modifiers. Journal of Controlled Release 2008;130:98–106. https://doi.org/10.1016/j.jconrel.2008.04.013.

[29] Madej M, Kurowska N, Strzalka-Mrozik B. Polymeric Nanoparticles—Tools in a Drug Delivery System in Selected Cancer Therapies. Applied Sciences (Switzerland) 2022;12. https://doi.org/10.3390/app12199479.

[30] Moloughney JG, Weisleder N. Poloxamer 188 (P188) as a Membrane Resealing Reagent in Biomedical Applications. vol. 6. 2012.

[31] Bashmail HA, Alamoudi AA, Noorwali A, Hegazy GA, Ajabnoor GM, Al-Abd AM. Thymoquinone enhances paclitaxel anti-breast cancer activity via inhibiting tumor-associated stem cells despite apparent mathematical antagonism. Molecules 2020;25. https://doi.org/10.3390/molecules25020426.

[32] Chou TC. Drug combination studies and their synergy quantification using the chou-talalay method. Cancer Res 2010;70:440–6. https://doi.org/10.1158/0008-5472.CAN-09-1947.

[33] Fu S, Chen X, Lo HW, Lin J. Combined bazedoxifene and paclitaxel treatments inhibit cell viability, cell migration, colony formation, and tumor growth and induce apoptosis in breast cancer. Cancer Lett 2019;448:11–9. https://doi.org/10.1016/j.canlet.2019.01.026.

[34] Czabotar PE, Lessene G, Strasser A, Adams JM. Control of apoptosis by the BCL-2 protein family: Implications for physiology and therapy. Nat Rev Mol Cell Biol 2014;15:49–63. https://doi.org/10.1038/nrm3722.

[35] Tait SWG, Green DR. Mitochondria and cell death: Outer membrane permeabilization and beyond. Nat Rev Mol Cell Biol 2010;11:621–32. https://doi.org/10.1038/nrm2952.

[36] Fessi H, Puisieux F, Devissaguet JP, Ammoury N, Benita S. Rapid Communication Nanocapsule formation by interfacial polymer deposition following solvent displacement. 1989.

[37] Cai J, Yue Y, Rui D, Zhang Y, Liu S, Wu C. Effect of chain length on cytotoxicity and endocytosis of cationic polymers. Macromolecules 2011;44:2050–7. https://doi.org/10.1021/ma102498g.

[38] Zolnik BS, González-Fernández A, Sadrieh N, Dobrovolskaia MA. Minireview: Nanoparticles and the Immune System. Endocrinology 2010;151:458–65. https://doi.org/10.1210/en.2009-1082.

[39] Budiman A, Nurani NV, Laelasari E, Muchtaridi M, Sriwidodo S, Aulifa DL. Effect of Drug–Polymer Interaction in Amorphous Solid Dispersion on the Physical Stability and Dissolution of Drugs: The Case of Alpha-Mangostin. Polymers (Basel) 2023;15:3034. https://doi.org/10.3390/polym15143034.

[40] Samaan TMA, Samec M, Liskova A, Kubatka P, Büsselberg D. Paclitaxel's mechanistic and clinical effects on breast cancer. Biomolecules 2019;9. https://doi.org/10.3390/biom9120789.

[41] Woo CC, Kumar AP, Sethi G, Tan KHB. Thymoquinone: Potential cure for inflammatory disorders and cancer. Biochem Pharmacol 2012;83:443–51. https://doi.org/10.1016/j.bcp.2011.09.029.

[42] Cüce-Aydoğmuş EM, İnhan-Garip GA. Investigation of the Effects of Blocking Potassium Channels With 4-Aminopyridine on Paclitaxel Activity in Breast Cancer Cell Lines. Cancer Rep 2024;7. https://doi.org/10.1002/cnr2.70072.

[43] Hochreiter-Hufford A, Ravichandran KS. Clearing the dead: Apoptotic cell sensing, recognition, engulfment, and digestion. Cold Spring Harb Perspect Biol 2013;5. https://doi.org/10.1101/cshperspect.a008748.

[44] Gascoigne KE, Taylor SS. Cancer Cells Display Profound Intra- and Interline Variation following Prolonged Exposure to Antimitotic Drugs. Cancer Cell 2008;14:111–22. https://doi.org/10.1016/j.ccr.2008.07.002.

[45] Taylor RC, Cullen SP, Martin SJ. Apoptosis: Controlled demolition at the cellular level. Nat Rev Mol Cell Biol 2008;9:231–41. https://doi.org/10.1038/nrm2312.

[46] Ma F, Li W, Liu C, Li W, Yu H, Lei B, et al. MiR-23a promotes TGF-β1-induced EMT and tumor metastasis in breast cancer cells by directly targeting CDH1 and activating Wnt/β-catenin signaling. 2017.

[47] Zhao X, Ma Y, Luo J, Xu K, Tian P, Lu C, et al. Blocking the WNT/β-catenin pathway in cancer treatment:pharmacological targets and drug therapeutic potential. Heliyon 2024;10. https://doi.org/10.1016/j.heliyon.2024.e35989.

[48] Peinado H, Olmeda D, Cano A. Snail, ZEB and bHLH factors in tumour progression: An alliance against the epithelial phenotype? Nat Rev Cancer 2007;7:415–28. https://doi.org/10.1038/nrc2131.

[49] Satelli A, Li S. Vimentin in cancer and its potential as a molecular target for cancer therapy. Cellular and Molecular Life Sciences 2011;68:3033–46. https://doi.org/10.1007/s00018-011-0735-1.

[50] Moorthi C, Krishnan K, Manavalan R, Kathiresan K. Preparation and characterization of curcumin-piperine dual drug loaded nanoparticles. Asian Pac J Trop Biomed 2012;2:841–8. https://doi.org/10.1016/S2221-1691(12)60241-X.

[51] Lv Y, He H, Qi J, Lu Y, Zhao W, Dong X, et al. Visual validation of the measurement of entrapment efficiency of drug nanocarriers. Int J Pharm 2018;547:395–403. https://doi.org/10.1016/j.ijpharm.2018.06.025.

[52] Deng X, Yang Z, Chan KW, Abu Bakar MZ. Exploring the Therapeutic Potential of 5-Fluorouracil-Loaded Calcium Carbonate Nanoparticles Combined with Natural Compound Thymoquinone for Colon Cancer Treatment. Pharmaceutics 2024;16:1011. https://doi.org/10.3390/pharmaceutics16081011.

[53] Feng LM, Wang XF, Huang QX. Thymoquinone induces cytotoxicity and reprogramming of EMT in gastric cancer cells by targeting PI3K/Akt/mTOR pathway. J Biosci 2017;42:547–54. https://doi.org/10.1007/s12038-017-9708-3.

[54] Akalın SA, Afşin Y, Özdemir İ, Tuncer MC, Öztürk Ş. Integrated Molecular Analysis of Thymoquinone–Methotrexate Synergy in Breast Cancer Cells: Apoptosis, Oxidative Stress, and Pathway Modulation. Pharmaceuticals 2025;18. https://doi.org/10.3390/ph18101551.

Supplementary Files

This is a list of supplementary files associated with this preprint. Click to download.

- TableS1.docx
- TableS2.docx